

Introduction to topological Phases in Condensed Matter

Adolfo G. Grushin¹

¹Univ. Grenoble Alpes, CNRS, Grenoble INP, Institut Néel, 38000 Grenoble, France

CONTENTS

I. Introduction	1	B. Kramers theorem	27
A. Why topological phases of matter	1	C. Pauli matrices	27
B. What is a topological insulator	2	D. Exact results for two-band Hamiltonians	27
C. Classification of topological phases	2	References	27
II. Recap: Second-quantization tight-binding Hamiltonians	2		
A. Example: 1D tight-binding chain	2		
B. General non-interacting second-quantized Hamiltonians	3		
C. Example 2: SSH and Rice-Mele model	3		
III. Symmetries	4		
A. Unitary Symmetries	4		
B. Non-unitary symmetries	5		
1. Time-reversal symmetry	6		
2. Particle-hole symmetry	7		
3. Chiral symmetry	8		
4. The 10-fold way	9		
IV. Phenomenology of topological phases from 1D examples: Su, Schrieffer and Heeger, Rice and Mele and Kitaev	9		
A. Topological properties of the Su-Schrieffer-Heeger (SSH) Model (1D)	9		
B. Polarization, Berry phase and Zak phase	11		
1. Quantized polarization as a topological invariant for the SSH model	11		
C. The invariant from inversion eigenvalues	12		
D. Edge States	13		
E. Edge states from the Dirac equation	15		
F. Wannier centers and charge pumping	15		
G. The SSH model and the 10-fold way	16		
H. 1D insulators are obstructed insulators	17		
I. Example II: Kitaev Wire	17		
V. Chern Insulators: Topological phases in 2D	18		
A. Chern Insulators and the Chern number	18		
B. Chern number and the Hall Conductivity	20		
C. Bulk-boundary correspondence: Chiral boundary modes	21		
D. 2D Quantum Spin-Hall insulators	22		
VI. 3D Topological Insulators in class AIII	25		
VII. Weyl semimetals	26		
VIII. Acknowledgements	27		
A. Useful relations	27		

Topological phases of matter are among the most robust phases of nature [1, 2]. Their many-body wavefunction cannot be described with purely localized orbitals, and the information that defines these phases is stored non-locally, spread over the entire system. Therefore, their physical properties, such as their metallic boundary states or quantized responses to external fields, are protected from local perturbations, such as defects, impurities, or other material imperfections.

The second defining characteristic is that they have fundamentally different responses to external perturbations (e.g. electromagnetic fields). Topological phases are defined by observables which depend only on combinations of fundamental constants, like e , h , or c , rather than on microscopic details, like the Fermi wave-vector, or the density of impurities. For example, the Hall conductivity of two-dimensional insulators is quantized by an integer times e^2/h .

Topological phases and properties are found in quantum systems like electrons in insulators [1, 2] and metals [3], ultra-cold atomic lattices, superconductors, or particle physics. They are also found in classical systems, like acoustic and photonic [4] metamaterials, mechanical systems [5] and even Earth's climate. In essence, any system that has a band structure can have topological phases. They can also occur in strongly interacting systems [6] of bosons, fermions, and even anyons (i.e. particles that, when exchanged, acquire an arbitrary phase $e^{i\theta}$ rather than a ± 1). Even systems without translational symmetry, like disordered systems and amorphous matter can be topological [7].

The classification of topological phases complements that of symmetry breaking. If you imagine a system of spins, these are disordered at high-temperatures by thermal fluctuations. At low temperatures they might order, say, into a ferromagnetic state, with all spins pointing up. The order parameter that captures the spontaneous breaking of rotational symmetry (the symmetry of the high-temperature state) is the local magnetization. Topological phases and cannot, by definition, be described by local order parameters.

B. What is a topological insulator

The basic property of an insulator is the absence of electrically conductive states. The simplest of all insulators is the atomic insulator, a set of disconnected atoms with electrons forming closed shells. If these atoms form a crystal lattice, we may use Bloch's theorem to combine these shells into energy bands separated by finite gaps. Since electrons are bound to the atoms they lack kinetic energy, and the bands $E_n(\mathbf{k})$ are exactly flat as a function of crystal momentum \mathbf{k} . Now imagine slowly bringing these atoms together, forming covalent bonds in the process. The electronic bands may now disperse with \mathbf{k} , and the gap sizes can change. If at all stages in the process we retained the existence of a band gap we may say that the two insulators, the atomic limit and the covalently bonded solid, are smoothly connected to each other by varying a parameter, in this case the strength of the covalent bonding. We call the insulators connected to the atomic insulator in this way topologically trivial insulators.

Topological insulators present fundamental obstructions to reach the atomic limit. The smooth process that connects them to the atomic insulator will always lead to a gap closing, and with it, fundamentally different responses. This defines topological insulators as insulators that cannot be smoothly transformed into an atomic limit. In many instances this obstruction is due to an underlying symmetry; there is no path that simultaneously keeps the gap open and respects the symmetry. For some insulators, the obstruction can be avoided by simply adding additional bands. These are called fragile topological insulators (one example is the Hopf insulator, which is only topologically sable if a system has exactly two bands).

C. Classification of topological phases

How can we classify topological phases? First we have to define the statistics of the particles we want to describe: are they fermions, bosons or anyons? The wave-function of two fermions (bosons) acquires a minus (plus) sign when we exchange two of these particles. Anyons when exchanged acquire a phase, or a matrix of phases. We will ignore anyons and bosons for the moment. Then we need to define whether the phase we want to describe is gapped or gapless. Gapped phases are topological insulators, while gapless topological phases are labeled topological metals. Lastly we need to specify if we are considering phases with long-range or short-range entanglement. I will ignore this latter distinction for the moment, until the end of the notes, but loosely speaking, long-range entangled phases require strong correlations between particles. These are generated by for example, strong Coulomb interactions (like in the Fractional quantum Hall effect).

Once this information is specified we will be asking three questions to classify our systems:

- What are the symmetries of the system?
- What is the system's dimensionality?

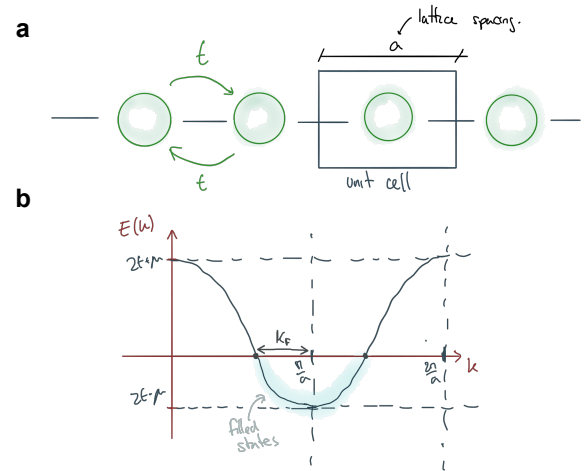


Figure 1. **a.** Lattice in real space with the unit cell. The lattice spacing is a and the hopping amplitude between nearest-neighbours is t . **b.** Dispersion relation resulting from Eq. (11).

- What are the possible topological phase that can exist given the above?

We start by a recap with tight-binding Hamiltonians, to which we will be asking these questions.

II. RECAP: SECOND-QUANTIZATION TIGHT-BINDING HAMILTONIANS

The Tight-Binding (TB) approximation relies on assuming that electrons hop from site to site with a given probability. In this approximation we do not really care where atoms are sitting precisely, we just care about the connectivity of the lattice and its symmetries. Lets set symmetries aside for the moment.

A. Example: 1D tight-binding chain

We want to write the Hamiltonian of an infinite 1D chain of L sites with spinless electrons hopping on it with an amplitude t (see Fig. 1a.). We need to define how electrons are created an annihilated at a given site i . This we do with the creation and annihilation operators c_i^\dagger and c_i that satisfy the commutation relations (12).

$$\{c_i, c_j^\dagger\} = \delta_{ij}, \quad \{c_i, c_j\} = \{\hat{\Psi}_i^\dagger, \hat{\Psi}_j^\dagger\} = 0 \quad (1)$$

They act on the space of occupation numbers, meaning they act on wavefunctions that look like $|n_1, n_2, \dots, n_N\rangle$ where n_i is the occupation number (how many particles are there) at a given site i . Thus creating an electron on site two of an empty lattice amounts to act with $c_2^\dagger |0, 0, 0, \dots, 0, 0\rangle = |0, 1, 0, \dots, 0, 0\rangle$, where an electron has been created at site i . Since we are considering a spinless problem, only one electron

is allowed per site. The electron operator acting on a given site i (I omit the site index) thus satisfy:

$$\hat{c}^\dagger|0\rangle = |1\rangle, \quad \hat{c}|0\rangle = 0, \quad (2)$$

$$\hat{c}^\dagger|1\rangle = 0, \quad \hat{c}|1\rangle = |0\rangle, \quad (3)$$

$$\hat{c}^\dagger\hat{c}|n\rangle \equiv \hat{n}|n\rangle = n|n\rangle, \quad n = 0, 1 \quad (4)$$

We have introduced the density operator \hat{n}_i which counts how many particles there are at a given site i . This type of operators act in what we called second-quantized basis. Don't care too much about the name (you can find more explanations in standard textbooks like Bruus and Flensberg [8]), it just means that instead of thinking about quantum mechanics as you learn in undergrad, it is more practical to think in terms of the "occupation" basis.

We are now in position to write our second-quantized Hamiltonian

$$H = \sum_i^L t\hat{c}_i^\dagger\hat{c}_{i+1} + t\hat{c}_{i+1}^\dagger\hat{c}_i + \mu\hat{n}_i \quad (5)$$

Here the first terms tells us how a particle hops from sites $i+1$ to i while the second tells us how it hops from i to $i+1$. Because the Hamiltonian needs to be hermitian, it is customary to not write the second term and just write *h.c.* for hermitian conjugate. The last term fixes the density of electrons at a chemical potential μ . Note that we have assumed that hopping terms between second neighbors and beyond are zero. For a periodic chain we can also rewrite the second term as

$$H = \sum_i^L t\hat{c}_i^\dagger\hat{c}_{i+1} + t\hat{c}_i^\dagger\hat{c}_{i-1} + \mu\hat{n}_i \quad (6)$$

Now we can use the translational symmetry of the chain to find the dispersion relation (Energy versus momentum \mathbf{k})

$$\hat{c}_i^\dagger = \frac{1}{\sqrt{L}} \sum_k e^{ikx_i} \hat{c}_k^\dagger \quad (7)$$

$$\hat{c}_i = \frac{1}{\sqrt{L}} \sum_k e^{-ikx_i} \hat{c}_k \quad (8)$$

with $k = 2\pi n/L$, which are the allowed momenta for a periodic lattice of length L . Introducing this into the Hamiltonian (6) and using that the lattice spacing is $x_{i+1} - x_i = a$ we get:

$$H = \frac{1}{L} \sum_{ikk'} t \left(e^{-i(k-k')x_i} e^{-ika} + e^{-i(k'-k)x_i} e^{ik'a} + \mu \right) \hat{c}_{k'}^\dagger \hat{c}_k \quad (9)$$

Using the completeness relation:

$$\sum_i e^{-i(k-k')x_i} = L\delta_{kk'} \quad (10)$$

we get

$$H = \sum_k E(k) \hat{c}_k^\dagger \hat{c}_k, \quad E(k) = 2t \cos(ka) + \mu \quad (11)$$

The dispersion relation is shown Fig. 1b.

The name of the (topological) game is to understand the symmetries of H and classify all possible phases. But I am getting ahead of myself. Before that note that in this example, to find the dispersion relation it was enough to express our chain in momentum space because we only had one degree of freedom (occupation: a site can either be empty or occupied).

B. General non-interacting second-quantized Hamiltonians

In general, non-interacting second-quantized Hamiltonians (including (5)) can be written as:

$$\hat{H} = \sum_{IJ}^N \hat{\Psi}_I^\dagger h_{IJ} \hat{\Psi}_J \quad (12)$$

in terms of the first-quantized (or single-particle) Hamiltonian h_{IJ} with operators that satisfy canonical commutation relations

$$\{\hat{\Psi}_I, \hat{\Psi}_J^\dagger\} = \delta_{IJ}, \quad \{\hat{\Psi}_I, \hat{\Psi}_J\} = \{\hat{\Psi}_I^\dagger, \hat{\Psi}_J^\dagger\} = 0 \quad (13)$$

The indices I and J encode all N degrees of freedom (e.g. site, orbital, spin...). For example, the single particle Hamiltonian for two sites with two spins corresponds to a 4×4 matrix h_{IJ} with I and J representing i, σ , and $i = 1, 2$ and $\sigma = \uparrow, \downarrow$.

For crystal systems a typical workflow is to express H in momentum space, which will leave us with a first-quantized Hamiltonian in momentum space $h_{IJ}(k)$. To obtain the eigenvalues $E_s(k)$ (the bands), where s runs over the number of degrees of freedom, we have to diagonalize $h_{IJ}(k)$. In our simple example, h_{IJ} was just a number, so no diagonalization was needed!

Next, an historically relevant example where h_{IJ} is a matrix.

C. Example 2: SSH and Rice-Mele model

The SSH model was conceived in 1979 by Su, Schrieffer and Bardeen to model polyacetylene a 1D carbon molecule [9]. As we will see, it is a nice model for topological phases in 1D.

Polyacetylene is a chain of carbon atoms. In it, the different carbon atoms are connected by two different bonds with hopping parameters $t(1 - \delta)$ and $t(1 + \delta)$ (see Fig. 2a). Thus we need a two site unit cell; we label the two carbon atoms in it A and B. The second-quantized Hamiltonian is

$$H = t \sum_{i=1}^L \left[(1 - \delta) c_{A,i}^\dagger c_{B,i} + (1 + \delta) c_{B,i}^\dagger c_{A,i+1} + h.c. \right] \quad (14)$$

The site index i no labels the unit-cell, and in each unit cell there are two types of atoms A and B. Again we go to momentum space using (7) and (8) such that

$$c_{\alpha,i} = \frac{1}{\sqrt{L}} \sum_k e^{i\vec{k} \cdot \vec{r}_i} c_{k,\alpha},$$

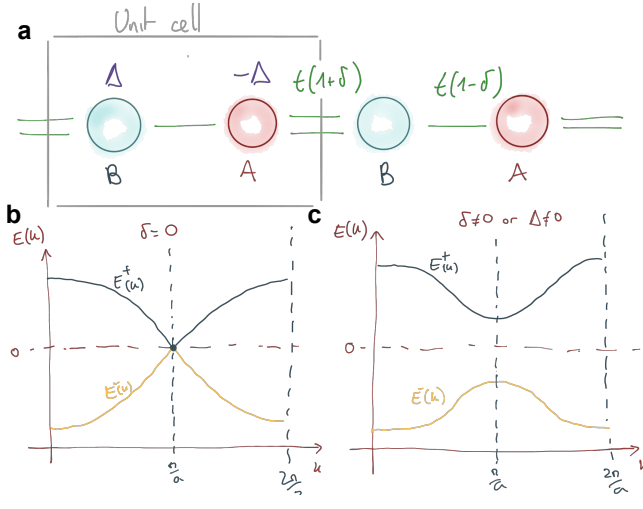


Figure 2. **a.** The SSH model has two types of hopping, strong and weak. When adding the extra on-site energy Δ it becomes the Rice-Mele Model. For a finite δ we say that the chain is dimerized. The corresponding dispersion relations without and with dimerization are shown in **b.** and **c.**

Note that here we need an extra index α to refer to orbitals A or B. The Hamiltonian can thus be rewritten in the form of (12) (in momentum space) as:

$$H = \sum_{\substack{k \in BZ, \\ \alpha \in A, B}} c_{\alpha, k}^\dagger h_{\alpha\beta}(k) c_{\beta, k}, \quad (15)$$

where (setting $t = 1$ for now on)

$$h_k^{\alpha\beta} = \begin{pmatrix} 0 & (1-\delta) + (1+\delta)e^{ika} \\ (1-\delta) + (1+\delta)e^{-ika} & 0 \end{pmatrix}$$

At this point we assume that the lattice spacing is $a = 1$, dropping it out of any further expressions. From your Algebra course you might remember that any Hermitian 2×2 matrix can be expressed in terms of Pauli matrices (σ_i , $i = x, y, z$) plus the 2×2 identity matrix (σ_0), because these four matrices are a complete basis. You can find them in Appendix D. Using them we can rewrite $h_k^{\alpha\beta}$ as

$$h_k^{\alpha\beta} = [(1-\delta) + (1+\delta)\cos k]\sigma_x + [(1+\delta)\sin k]\sigma_y + 0 \cdot \sigma_z + 0 \cdot \mathbb{1} \quad (16)$$

$$\equiv \vec{d}_k \cdot \vec{\sigma} + \varepsilon_k \sigma_0 \quad (17)$$

where we $\varepsilon_k = 0$ in this example and we have defined a vector

$$\vec{d}_k = ((1-\delta) + (1+\delta)\cos k, (1+\delta)\sin k, 0).$$

Diagonalizing this Hamiltonian is analytically possible for any \vec{d}_k and ε_k and results in two bands

$$E_k^\pm = \pm |\vec{d}_k| + \varepsilon_k. \quad (18)$$

For our particular case this reads

$$\begin{aligned} E_k^\pm &= \pm \sqrt{d_x^2 + d_y^2 + d_z^2} + \varepsilon_k \\ &= \pm \sqrt{((1-\delta) + (1+\delta)\cos k)^2 + ((1+\delta)\sin k)^2} + \varepsilon_k \end{aligned} \quad (19)$$

The bands are shown in Fig. 2b and c. When $\delta = 0$ there is no energy for which we do not cross a gap, so the model is gapless. For finite δ the model is dimerized and the bands become gapped.

One more thing. Note that if we would have added an onsite energy for the A and B sites of m and $-m$ respectively this would have introduced a term

$$H_m = m \sum_{i=1}^L [c_{A,i}^\dagger c_{A,i} - c_{B,i}^\dagger c_{B,i}] \quad (20)$$

The SSH Hamiltonian plus H_m are known as the **Rice-Mele model**, and is a classical model of 1D semiconductors with broken inversion symmetry (you will see why later on).

If we proceed as before H_m would have added a σ_z term in $h_k^{\alpha\beta}$

$$h_k^{\alpha\beta} = [(1-\delta) + (1+\delta)\cos k]\sigma_x + [(1+\delta)\sin k]\sigma_y + m/t \cdot \sigma_z + 0\sigma_0 \quad (21)$$

Thus $\varepsilon_k = 0$ and

$$\vec{d}_k = ((1-\delta) + (1+\delta)\cos k, (1+\delta)\sin k, m).$$

A finite Δ results in a gap too, which you can check by plotting the updated bands

$$\begin{aligned} E_k^\pm &= \pm \sqrt{d_x^2 + d_y^2 + d_z^2} + \varepsilon_k \\ &= \pm \sqrt{((1-\delta) + (1+\delta)\cos k)^2 + ((1+\delta)\sin k)^2 + m^2} \end{aligned} \quad (22)$$

However, we will see that the symmetry properties of a Hamiltonian with only δ or only m are very different! So lets learn how to deal with symmetries.

III. SYMMETRIES

The concept of symmetry is deeply rooted in our understanding of condensed matter, and topological insulators and metals are not an exception. Although topological phases can exist in the absence of any symmetry, symmetry enriches their classification, and allows to express the topological invariants that define these phases and their responses in mathematically simple ways. We first give a bit of background and then review unitary and non-unitary symmetries.

A. Unitary Symmetries

Perhaps without noticing, you have already seen an example of unitary symmetry, which is the invariance under lattice

translations, which allowed us to write (7) and (8). We decomposed H into different "Hamiltonian blocks", one for each k . For the 1D chain these blocks were one-dimensional, and thus we diagonalized the Hamiltonian. For the SSH and Rice-Mele models, each k -block was two-dimensional, and thus we still had to diagonalize it further.

This is a general thing that happens with unitary symmetries: If your Hamiltonian is symmetric (we will formalize this in shortly) you can find a basis where it can be expressed as a Block diagonal matrix.

Consider a fermionic system described by general second-quantized Hamiltonian, H (12) and canonical relations (13). A system is symmetric under the action of a unitary symmetry if 1) the canonical commutation relations are preserved and 2) the Hamiltonian matrix in second-quantization commutes with the unitary matrix that represents the symmetry.

A unitary symmetry is a symmetry that changes the fermionic operators with a unitary matrix such that

$$\hat{\Psi}_I \rightarrow \hat{\Psi}'_I = \sum_J U_{IJ} \hat{\Psi}_J \equiv \hat{U} \hat{\Psi}_I \hat{U}^{-1} \quad (23)$$

$$\hat{\Psi}_I^\dagger \rightarrow \hat{\Psi}'_I^\dagger = \sum_J \hat{\Psi}_J^\dagger U_{IJ}^* \equiv \hat{U} \hat{\Psi}_I^\dagger \hat{U}^{-1} \quad (24)$$

By asking that (13) are preserved under this transformation we demand that $\{\hat{\Psi}_I, \hat{\Psi}_J^\dagger\} = \hat{U}\{\hat{\Psi}_I, \hat{\Psi}_J^\dagger\}\hat{U}^{-1}$, which implies that U_{IJ} is a unitary matrix ($UU^\dagger = \mathbb{1}$).

By asking that the Hamiltonian commutes with U , $\hat{U} \hat{H} \hat{U}^{-1} = \hat{H}$, we arrive that the single particle Hamiltonian must satisfy $U^\dagger h U = h$.

When U acts on the spatial indices i, j we call it a spatial unitary symmetry (e.g. lattice rotations, inversions, mirrors,...). When U acts on other degrees of freedom we call it non-spatial unitary transformation. For example, in the special case where U acts equally on every site, $U = \prod_i U_i$, U is a non-spatial on-site unitary symmetry (e.g. the unitary symmetry that flips a spin on each site is $U = \prod_i \sigma_x^i$).

When a unitary matrix is a symmetry, it commutes with the second-quantized Hamiltonian H . Thus we can find a basis where both H and U are block diagonal. Each block is called an irreducible representation (irrep) of the symmetry. This block has a common symmetry eigenvalue (colors). Note irreps do not necessary have the same dimension.

a. *Example: Translation symmetry.* As mentioned above, when H is translationally symmetric (we have a periodic lattice), each block corresponds to a value of k . If we have no internal degrees of freedom, like in our simpler tight-binding chain example, each block is one dimensional. If there are more than degrees of freedom per site then each block is higher dimensional.

b. *Example: Inversion symmetry.* Let's show that inversion \hat{I} is a unitary operator. First we consider how it acts upon the position and momentum operators,

$$\hat{I}\hat{x}\hat{I}^{-1} = -\hat{x}$$

$$\hat{I}\hat{p}\hat{I}^{-1} = -\hat{p}$$

$$\hat{I}[\hat{x}, \hat{p}]\hat{I}^{-1} = Ii\hbar I^{-1}$$

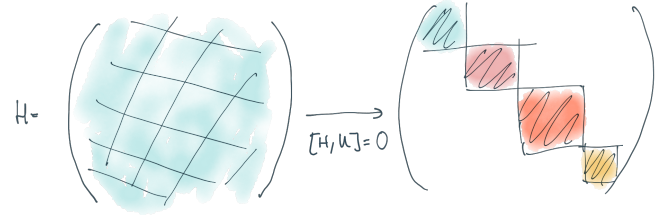


Figure 3. A unitary symmetry diagonalizes the Hamiltonian in Blocks.

The first relation is by definition inversion: inversion is the operation that flips all spatial coordinates. The second relation can be intuitively understood from the fact that momentum must transform as a velocity. Since velocity is a time derivative of the position operator, which picks up a minus sign, momentum must also pick up a minus sign under inversion. Finally, in the third line we have applied inversion at both sides of the uncertainty principle. We notice that for the left hand side to be equal to the right-hand side inversion must be a unitary operator: $\hat{I}^\dagger \hat{I} = \mathbb{1}$. This is because Wigner showed that unitary operators do not complex conjugate the quantity they act on. This is unlike anti-unitary operator can always be represented as a unitary matrix times complex conjugation UK .

Now lets see how inversion acts on a simple example: a molecule with two atoms with electrons hopping between them. In this case H is a two-dimensional matrix

$$h = \begin{pmatrix} 0 & t \\ t & 0 \end{pmatrix} = t\sigma_x.$$

The eigenvalues are $E = \pm t$ and eigenfunctions are $|\psi_\pm\rangle = (\pm 1, 1)$. Inversion interchanges the two atoms from the center, and thus it is represented by $\hat{I} = \sigma_x$, so $[h, \sigma_x] = 0$. Notice then that $|\psi_\pm\rangle$ are even and odd under inversion. Using the eigenvectors, we can construct a matrix U_D (U_D has the eigenvectors as columns) to write h in a diagonal basis $h' = U_D^\dagger h U_D = -t\sigma_z$, where the upper (lower) block, which is one-dimensional, is odd (even) under inversion.

B. Non-unitary symmetries

Unitary operators separate H in blocks. If we block diagonalize H by using all unitary transformations allowed by the symmetries of H and examine one of the block-diagonalized

sections, we have exhausted all of the unitary, commuting operations. But what can we say about the blocks themselves? We found unitary matrices that commute with the Hamiltonian, but we can find antiunitary matrices that either commute or anticommute with the single-particle blocks of h . These cases correspond to time-reversal symmetry and particle-hole (charge-conjugation) symmetry. Their combination will form a matrix that is unitary but anticommutes with h , which we call chiral (or sometimes sublattice) symmetry. It is possible to show [10] that these possibilities are exhaustive and lead to 10 possibilities, which lead to 10 different classes of *strong* topological phases.

1. Time-reversal symmetry

By definition the time-reversal symmetry operator as

$$\hat{T} : t \rightarrow -t. \quad (25)$$

Its action on the position and momentum operators, we observe

$$\hat{T}\hat{x}\hat{T}^{-1} = \hat{x} \quad (26)$$

$$\hat{T}\hat{p}\hat{T}^{-1} = -\hat{p}. \quad (27)$$

When we apply these to the uncertainty principle we find

$$\hat{T}i\hbar\hat{T}^{-1} = \hat{T}[\hat{x}, \hat{p}]\hat{T}^{-1} = -[\hat{x}, \hat{p}] = \quad (28)$$

which implies that we should have

$$\hat{T}i\hat{T}^{-1} = -i. \quad (29)$$

From this last equation, we need to demand that \hat{T} is expressed as a combination of a unitary matrix and complex conjugation, i.e. time-reversal is anti-unitary:

$$\hat{T} = \hat{U}_T \mathcal{K} \quad (30)$$

For \hat{T} to be a symmetry it commutes with H in second quantization $\hat{T}\hat{H}\hat{T}^{-1} = \hat{H}$. Its action on the Fermionic operators is [11]

$$\hat{\Psi}_I \rightarrow \hat{\Psi}'_I = \sum_J (U_T)_{IJ} \hat{\Psi}_J \quad (31)$$

From $\hat{T}\hat{H}\hat{T}^{-1} = \hat{H}$ we can derive its action on the first quantized Hamiltonian:

$$U_T^\dagger h^* U_T = h \quad (32)$$

Note that if an operator \hat{O} is preserved under \hat{T} , we have $\hat{T}\hat{O}(t)\hat{T}^{-1} = \hat{T}e^{i\hat{H}t}\hat{O}(t)e^{-i\hat{H}t}\hat{T}^{-1} = \hat{O}(-t)$. The condition on the first quantized hamiltonian is then

Because of its anti-unitary nature, time-reversal can square to ± 1 . To see this, we can consider the difference between the

time-reversal operator acting on spinful and spinless particles. Let's examine \hat{T} acting on a spin matrix, \vec{S} . By definition spin is like an angular momentum. Any angular momenta \vec{L} transform like the vector product of \vec{x} and \vec{p} . Because of (26) \vec{L} , and thus \vec{S} has to change sign with time reversal, and we have

$$\hat{T}\vec{S}\hat{T}^{-1} = -\vec{S} \quad (33)$$

We can represent this action by a rotation around an axis, say y and complex conjugation[12]. A rotation by π around the y axis is represented by the operator $e^{-i\pi S_y}$ thus leading to $\hat{T} = e^{-i\pi S_y} \mathcal{K}$. For spin-1/2 particles, $\vec{S} = \frac{1}{2}(\sigma_x, \sigma_y, \sigma_z)$. Therefore $\hat{T} = e^{-i\pi\sigma_y/2} \mathcal{K} = -i\sigma_y \mathcal{K}$ [13]. Note that in this case $T^2 = -1$. However, if we consider particles without spin ($S = 0$), it is sufficient to take $\hat{T} = \mathcal{K}$ (there is no rotation needed!) and $T^2 = 1$.

There is a fundamental difference between the two possibilities $T^2 = \pm 1$ which is that for $T^2 = -1$ we have Kramers theorem: under time-reversal symmetry we have doublets of time-reversed states with the same energy, E . To prove it [14], start we proceed by contradiction (a different, perhaps more rigorous proof [12] is given in Appendix B). First, lets assume that $|\psi\rangle$ and $\hat{T}|\psi\rangle$ are the same state. Thus, they can only differ by a phase $\hat{T}|\psi\rangle = e^{i\phi}|\psi\rangle$. We want to show that they are a different state, so apply \hat{T} again, resulting in $\hat{T}^2|\psi\rangle = \hat{T}e^{i\phi}|\psi\rangle = e^{-i\phi}\hat{T}|\psi\rangle$. Using our assumption that $T|\psi\rangle = e^{i\phi}|\psi\rangle$ on the right hand side we obtain $\hat{T}^2|\psi\rangle = e^{-i\phi}e^{i\phi}|\psi\rangle = |\psi\rangle$. This is a contradiction because we assumed that $\hat{T}^2 = -1$!. Thus $T|\psi\rangle$ and $|\psi\rangle$ must be different states. However they have the same energy. We remember that H and T commute, $[H, T] = 0$, so we can change the order of H and T and obtain

$$HT|\psi\rangle = TH|\psi\rangle = TE|\psi\rangle. \quad (34)$$

Therefore, given a system, there are three possibilities: time-reversal is not a symmetry, time-reversal is a symmetry with $\hat{T}^2 = 1$, or time-reversal is a symmetry with $\hat{T}^2 = -1$. We have six different possibilities, presented in Table I.

time-reversal is	\hat{T}	T^2
Absent	0	x
Present	+1	+1
Present	-1	-1

Table I. Possibilities of time-reversal symmetries in a system. Usually we only show the central column.

Lastly it is useful to determine what condition does time-reversal impose on a first-quantized Hamiltonian in momentum space $h(\mathbf{k})$. Consider the general second-quantized Hamiltonian in momentum space (13),

$$H = \sum_k c_{k,\alpha}^\dagger h_k^\beta c_{k,\beta}, \quad (35)$$

where k corresponds to momentum and α, β can label orbitals (but not spin!). Now we need to understand what is the action of time reversal on

$$\hat{T}c_{\alpha,i}\hat{T}^{-1} = \frac{1}{\sqrt{L}} \sum_k e^{-i\vec{k}\cdot\vec{r}_i} \hat{T}c_{k,\alpha}\hat{T}^{-1} \quad (36)$$

$$= \frac{1}{\sqrt{L}} \sum_k e^{i\vec{k}\cdot\vec{r}_i} \hat{T}c_{-k,\alpha}\hat{T}^{-1}, \quad (37)$$

Note in the last line we changed $k \rightarrow -k$. Now we apply this to the full Hamiltonian:

$$H = \hat{T}H\hat{T}^{-1} = \sum_k c_{-k,\alpha}^\dagger \hat{T}h_k^\beta \hat{T}^{-1} c_{-k,\beta}, \quad (38)$$

which implies that the first quantized hamiltonian has to satisfy:

$$\hat{T}h_k\hat{T}^{-1} = h_{-k}. \quad (39)$$

Using that \hat{T} is an antiunitary operator:

$$U_T h_k^* U_T^\dagger = h_{-k}. \quad (40)$$

where U_T is unitary ($U_T U_T^\dagger = \mathbb{1}$).

We have to note that if the particles are spinful $c_{\alpha,i,\sigma}$, with $\sigma = \uparrow, \downarrow$ transforms a bit differently (see [12]):

$$\hat{T}c_{i\uparrow}\hat{T}^{-1} = c_{i\downarrow}, \quad (41)$$

$$\hat{T}c_{i\downarrow}\hat{T}^{-1} = -c_{i\uparrow}. \quad (42)$$

We are now ready to check some examples:

a. *Example: Zeeman field* The Hamiltonian of a spin-1/2 in a magnetic field is $h = \vec{B} \cdot \vec{\sigma}$. We can check if this is time-reversal symmetric by using $\hat{T} = -i\sigma_y\mathcal{K}$ and:

$$\hat{T}h\hat{T}^{-1} = -\vec{B} \cdot \vec{\sigma} \neq h \quad (43)$$

As it should (see Eq. 33), h is not time-reversal symmetric because a magnetic field breaks time-reversal symmetry. Think of a loop of current created by a magnetic field, and reverse the arrow of time. The current rotates in the opposite direction, as if the magnetic field was reversed.

b. *Example: Graphene* Consider a Hamiltonian:

$$H = k_x\sigma_x + k_y\sigma_y \quad (44)$$

This can be spinless graphene's Hamiltonian around one valley. Then, taking $\hat{T} = \mathbb{1}\mathcal{K}$ we have

$$\mathcal{K}h\mathcal{K} = k_x\sigma_x - k_y\sigma_y \neq h_{-k} \quad (45)$$

Time-reversal takes us to another Hamiltonian, which happens to be the Hamiltonian around the other Valley. Thus, a single valley in graphene breaks time-reversal, but considering the two valleys will result in a time-reversal symmetric Hamiltonian. This is physically reasonable because pristine graphene does not break time-reversal symmetry.

c. *Example: Surface state of a time-reversal invariant topological insulator* Consider the same Hamiltonian:

$$H = k_x\sigma_x + k_y\sigma_y \quad (46)$$

but now σ encodes the real spin. Then we need to take $\hat{T} = -i\sigma_y\mathcal{K}$ and thus we have

$$Th_k\hat{T}^{-1} = -i\sigma_y\mathcal{K}h_ki\sigma_y\mathcal{K} = \sigma_y h_k^* \sigma_y \quad (47)$$

$$= \sigma_y(k_x\sigma_x - k_y\sigma_y)\sigma_y \quad (48)$$

$$= -k_x\sigma_x - k_y\sigma_y = h_{-k} \quad (49)$$

where we have used that $\mathcal{K}^2 = 1$, $\{\sigma_i, \sigma_j\} = \sigma_i\sigma_j + \sigma_j\sigma_i = \delta_{ij}$ and $\sigma_i^2 = \mathbb{1}$. In this case the Hamiltonian is time-reversal invariant because it satisfies (39).

2. Particle-hole symmetry

We can play a similar game with the symmetry that turns creating particles into creating holes (annihilating particles) [11]

$$\Psi_I \rightarrow \Psi'_I = (U_C)_{IJ}^* \Psi_J^\dagger \equiv \hat{C}\Psi_I \hat{C}^{-1} \quad (50)$$

\hat{C} is also called charge-conjugation because it flips σ . Again, demanding that the commutation relations are preserved we find that U_C is unitary. Demanding that the second-quantized Hamiltonian is invariant results in a condition for the single particle hamiltonian:

$$U_C^\dagger h^* U_C = -h \quad (51)$$

Therefore, from the perspective of h , the particle-hole operator is an anti-unitary operator ($C = UK$) that anti-commutes with the Hamiltonian. Therefore, there are again two cases depending on whether $C^2 = \pm 1$.

Following as before, it is possible to show that

1. For particle-hole symmetric $H = \hat{C}H\hat{C}^{-1}$, if $|\phi\rangle$ is an eigenstate, so is $\hat{C}|\phi\rangle$ and

2. For every single-particle eigenstate at energy ϵ , there is a particle-hole reversed eigenstate with energy $-\epsilon$.

$$\begin{aligned} h|\psi\rangle &= \epsilon|\psi\rangle \\ h(\hat{C}|\psi\rangle) &= -\hat{C}h|\psi\rangle \\ &= -\epsilon(\hat{C}|\psi\rangle) \end{aligned}$$

This operator has a classification table similar to that of time-reversal symmetry, as shown in Table III.

particle-hole symmetry is	\hat{C}	\hat{C}^2
Absent	0	-
Present	+1	+1
Present	-1	-1

Table II. Possibilities of particle-hole symmetry for a given system.

Following similarly as for Time-reversal symmetry we can show that, in momentum space, the single-particle Hamiltonian satisfies

$$Ch_k C^{-1} = -h_{-k} \quad (52)$$

or

$$U_C h_k^* U_C^\dagger = -h_{-k} \quad (53)$$

a. *Example: BdG Hamiltonians for superconductors have particle-hole symmetry by definition* In second-quantized Hamiltonians of superconductors we have to deal with pairing terms, i.e. like $\frac{\Delta}{2}(c^\dagger c^\dagger + cc)$. Hence, a second-quantized Hamiltonian with pairing terms can be written in general as

$$\begin{aligned} H = & \sum_{IJ}^N \hat{\Psi}_I^\dagger h_{IJ} \hat{\Psi}_J + \\ & + \frac{1}{2} \sum_{IJ}^N \hat{\Psi}_I^\dagger \Delta_{IJ} \hat{\Psi}_J^\dagger + \hat{\Psi}_I \Delta_{IJ}^* \hat{\Psi}_J. \end{aligned} \quad (54)$$

The first line is the typical second-quantized Hamiltonian and the second line are superconducting pairing terms. It is convenient to write the second quantized Hamiltonian using a Nambu spinor which is a combination of particles Ψ_I^\dagger and holes Ψ_I :

$$\hat{\chi}^\dagger \equiv (\hat{\Psi}_1^\dagger \cdots \hat{\Psi}_N^\dagger, \hat{\Psi}_1 \cdots \hat{\Psi}_N) \quad (55)$$

Using (55) we can write H , which is known as the Bogoliubov de Gennes (BdG) Hamiltonian, as

$$H_{\text{BdG}} = \frac{1}{2} \sum_{AB}^{2N} \hat{\chi}_A^\dagger h_{AB}^{\text{BdG}} \hat{\chi}_B \quad (56)$$

where A, B now run over $2N$ degrees of freedom and the first-quantized BdG is defined as

$$h^{\text{BdG}} = \begin{pmatrix} h & \Delta \\ \Delta^* & -h^T \end{pmatrix}$$

where $h = h^\dagger$ by Hermiticity of the Hamiltonian and $\Delta = -\Delta^T$ by Fermi-statistics. Here comes the important part: while $\hat{\Psi}$ and $(\hat{\Psi}^\dagger)^T$ are independent, $\hat{\chi}$ and $(\hat{\chi}^\dagger)^T$ are not:

$$(\hat{\chi}^\dagger)^T = \begin{pmatrix} (\hat{\Psi}^\dagger)^T \\ \hat{\Psi} \end{pmatrix} = \tau_x \begin{pmatrix} \hat{\Psi} \\ (\hat{\Psi}^\dagger)^T \end{pmatrix} = \tau_x \hat{\chi} \quad (57)$$

and similarly $\hat{\chi}^\dagger = \hat{\chi}^T \tau_x$ with

$$\tau_x = \begin{pmatrix} 0_N & 1_N \\ 1_N & 0_N \end{pmatrix},$$

being the x Pauli matrix acting in particle-hole space with $N \times N$ blocks. Now, we can check what this property does to

our Hamiltonian:

$$H_{\text{BdG}} = \frac{1}{2} \sum_{AB}^{2N} \hat{\chi}_A^\dagger h_{AB}^{\text{BdG}} \hat{\chi}_B \quad (58)$$

$$= \frac{1}{2} \sum_{ABCD}^{2N} \hat{\chi}_C(\tau_x)_{CA} h_{AB}^{\text{BdG}}(\tau_x)_{BC} \hat{\chi}_D^\dagger \quad (59)$$

$$= \frac{1}{2} \sum_{AB}^{2N} \hat{\chi}_A(\tau_x h^{\text{BdG}} \tau_x)_{AB} (\hat{\chi}_B^\dagger)_B \quad (60)$$

$$= \frac{1}{2} \sum_{AB}^{2N} (\tau_x h^{\text{BdG}} \tau_x)_{AB} (-\hat{\chi}_B^\dagger \hat{\chi}_A + \delta_{AB}) \quad (61)$$

$$\begin{aligned} &= -\frac{1}{2} \sum_{AB}^{2N} \hat{\chi}_B^\dagger ((\tau_x h^{\text{BdG}} \tau_x)_{BA})^T \hat{\chi}_A \\ &+ \text{Tr}(\tau_x h^{\text{BdG}} \tau_x) \end{aligned} \quad (62)$$

By definition of the first-quantized BdG Hamiltonian, the term with the trace is zero, and we have:

$$\tau_x h_{\text{BdG}}^t \tau_x = \tau_x h_{\text{BdG}}^* \tau_x = -h_{\text{BdG}} \quad (63)$$

Therefore, any BdG Hamiltonian has, by definition, particle-hole symmetry.

3. Chiral symmetry

Lastly there is the possibility of having a combination of both time-reversal and particle-hole symmetry to form the so called chiral symmetry operator, $\hat{S} = \hat{C} \cdot \hat{T}$ (the alternative definition $\hat{S} = \hat{T} \cdot \hat{C}$ amounts to a change of basis of the Hamiltonian). In the space of \hat{H} it is also an anti-unitary symmetry that commutes with the Hamiltonian [10]

$$\hat{S} H \hat{S}^{-1} = H \quad (64)$$

However, in first quantized space it is a unitary operator that anti-commutes with the single-particle hamiltonian

$$\begin{aligned} S = U_S &\equiv U_T \mathcal{K}(U_C \mathcal{K}) = U_T (U_C)^* \\ U_S h U_S^\dagger &= -h \\ U_S h_k U_S^\dagger &= -h_k \quad (\text{momentum space}) \end{aligned}$$

S is unitary and always squares to $S^2 = 1$ [10] so there are only two possibilities

chiral symmetry is	\hat{C}	\hat{C}^2
Absent	0	-
Present	+1	+1

Table III. Possibilities of chiral symmetry for a given system.

Lastly, as happened with particle-hole symmetry the single-particle spectrum comes in $\epsilon, -\epsilon$ pairs:

$$\begin{aligned} h|\psi\rangle &= \epsilon|\psi\rangle \\ h(S|\psi\rangle) &= -Sh|\psi\rangle \\ &= -\epsilon(S|\psi\rangle) \end{aligned}$$

Specifically an zero-energy state is doubly degenerate.

4. The 10-fold way

When we combine all of the possibilities of these three different symmetries (we can show that they are exhaustive [10]), we wind up with a big table as shown in Table IV.

\hat{T}	\hat{C}	\hat{S}
± 1	± 1	1
± 1	∓ 1	1
± 1	0	0
0	± 1	0
0	0	1
0	0	0

Table IV. 10-fold classification of non-unitary symmetries

This table is known as the ten-fold way or ten-fold classification. Depending on the dimensionality we will find different systems have different topological properties depending on their symmetry.

IV. PHENOMENOLOGY OF TOPOLOGICAL PHASES FROM 1D EXAMPLES: SU, SCHRIEFFER AND HEEGER, RICE AND MELE AND KITAEV

As a summary of the previous lecture, considering that spatial symmetries are unitary and block diagonalize the Hamiltonian, we need to consider three non-spatial symmetries: time-reversal, particle-hole and chiral symmetries. Here is a reminder of how they act in momentum-space on the first-quantized Hamiltonian h :

Time-reversal symmetry: anti-unitary, commuting:

$$Th_kT^{-1} = h_{-k}, \quad T = U_T \mathcal{K} \quad (65)$$

Particle-hole symmetry: anti-unitary, anti-commuting:

$$Ch_kC^{-1} = -h_{-k}, \quad C = U_C \mathcal{K} \quad (66)$$

Chiral symmetry: unitary, anti-commuting):

$$Sh_kS^{-1} = -h_k, \quad S = U_S \quad (67)$$

All of the different possible combinations of the presence or absence of these symmetries (and in the case of time-reversal and particle-hole the sign of the operator squared) leads us to 10 different possibilities.

Spatial symmetries will be also important, especially when considering crystalline topological insulators. It is useful to

recall the action of inversion on in momentum space:

$$\text{Inversion (unitary, commuting)}: \quad I h_k I^{-1} = h_{-k} \quad (68)$$

which follows from how a general unitary spatial symmetry acts on a single-particle hamiltonian:

$$U_G h(k) U_G^\dagger = h(u_G k) \quad (69)$$

where u_G is a matrix that acts on the momentum as indicated by the symmetry; $k \rightarrow -k$ in the case of inversion (see Ref. [11] for more details).

Now that we know how to handle symmetries we are going to see how different insulators with the same symmetry are classified by topological invariants. We will be guided by two principles

- **Adiabatic principle:** As explained in the introduction previous section gapped phases that can be smoothly connected to each other by changing the paramters of the Hamiltonian but not changing the gap will be in the same topological phase.
- **Locality:** The terms we are allowed to add to the Hamiltonian are local.

These restrict our discussion to zero temperature ground-states of local Hamiltonians. This does not mean that topological states cannot be defined out of equilibrium or for non-local Hamiltonians, but this is too advanced for the moment. We know will systematically go from 1D to 2D and 3D given examples of the type of phases that we can encounter in different symmetry classes. We start with the SSH model that we already introduced above. Although we will see 1D is quite special, this model allows to exemplify many of the common properties of topological insulators.

A. Topological properties of the Su-Schrieffer-Heeger (SSH) Model (1D)

From Section II C we recall that the Hamiltonian in momentum space of the SSH model is

$$h_k = \vec{d}_k \cdot \vec{\sigma} + \varepsilon_k \sigma_0 \quad (70)$$

where we $\varepsilon_k = 0$ and

$$\vec{d}_k = \left((1 - \delta) + (1 + \delta) \cos k, (1 + \delta) \sin k, 0 \right). \quad (71)$$

Diagonalizing this Hamiltonian is analytically possible for any \vec{d}_k and ε_k and results in two bands

$$E_k^\pm = \pm |\vec{d}_k| + \varepsilon_k. \quad (72)$$

Since we are interested in gapped systems we ask when is $|\vec{d}_k| \neq 0$ satisfied (the condition for the absence of energy levels). From (71), $d_z = 0$ for all k . This implies that the Hamiltonian is gapped for all \vec{d}_k so long as we don't hit the origin $\vec{d} = (0, 0, 0)$. Here we can notice something

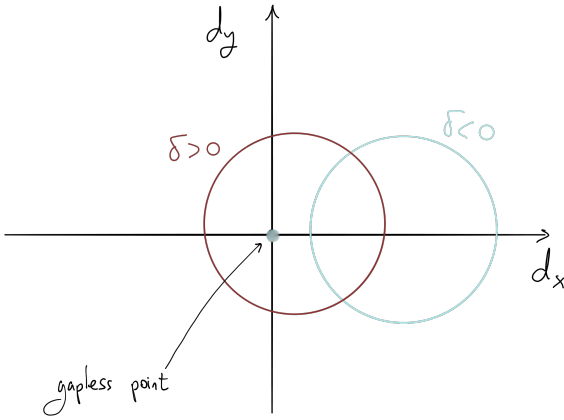


Figure 4. Two different paths in parameter space. If we keep $\delta > 0$ and change k we will encircle the origin, while if we keep $\delta < 0$ and change k we will not encircle the origin. These two insulators are thus only connected by a gapless phase transition, so long as $d_z = 0$.

interesting. Depending on the value of δ , as we move in k , we either will encircle or not the origin if we draw a closed path in the (d_x, d_y) plane. This means there are two different type of insulators which we can connect only by passing through a gapless point. Note that this statement relies on the fact that $d_z = 0$ because if not the drawing above has a third axes, allowing us to connect the two paths avoiding the origin.

So, if $d_z = 0$ is what is needed, we need a symmetry that can impose it. It turns out there are several ways of imposing this, here we consider two.

- **Chiral symmetry:** Remember that a σ_z term in the SSH Hamiltonian was generated by a term like the Rice-Mele mass (20). We might then consider the restrictions imposed by the unitary chiral symmetry (from (67) we have $U_S d_k U_S^\dagger = -h_k$) with $U_S = \sigma_z$. Consider how U_S acts on a general 2×2 Hamiltonian

$$h_k = d_k^x \sigma_x + d_k^y \sigma_y + d_k^z \sigma_z + \varepsilon_k \sigma_0 \quad (73)$$

such that

$$U_S d_k U_S^\dagger = \sigma_z (d_k^x \sigma_x + d_k^y \sigma_y + d_k^z \sigma_z + \varepsilon_k \sigma_0) \sigma_z \quad (74)$$

$$= -d_k^x \sigma_x - d_k^y \sigma_y + d_k^z \sigma_z + \varepsilon_k \sigma_0 \quad (75)$$

We see that if this is to be equal to $-h_k$, chiral symmetry $S = \sigma_z$ imposes that both $d_k^z = -d_k^z$ and $\varepsilon_k = -\varepsilon_k$, which have thus to vanish. So indeed chiral symmetry is enough to impose $d_k^z = 0$ (and $\varepsilon_k = 0$!). This symmetry forbids terms like $c_{A,i}^\dagger c_{A,i}$ or $c_{B,i}^\dagger c_{B,i}$.

- **Inversion and Time-reversal symmetry:** Since we are dealing with spinless fermions, time-reversal symmetry

is implemented by complex-conjugation $\hat{T} = \mathcal{K}$. Recalling that in this case $U_T = \mathbb{1}$ and thus, from (65), $h_k^* = h_{-k}$ and time-reversal imposes on (73) that

$$d_k^x = d_{-k}^x \quad (76)$$

$$d_k^y = -d_{-k}^y \quad (77)$$

$$d_k^z = d_{-k}^z \quad (78)$$

$$\varepsilon_k = \varepsilon_{-k} \quad (79)$$

While our SSH Hamiltonian satisfies these symmetries, (it is time-reversal invariant!) time-reversal alone is not enough to impose $d_z(k) = 0$. For that we need an extra symmetry which in this case is inversion.

As we saw, inversion sends x to $-x$. Choosing our center of inversion as the center point on the bond between the A and B sites it corresponds to sending A to B . The matrix that does that for us, in A, B space is σ_x :

$$\sigma_x \hat{c} = \begin{pmatrix} 0 & 1 \\ 1 & 0 \end{pmatrix} \begin{pmatrix} \hat{c}_A \\ \hat{c}_B \end{pmatrix} = \begin{pmatrix} \hat{c}_B \\ \hat{c}_A \end{pmatrix}. \quad (80)$$

from (68), we thus have the constraint imposed by inversion $\sigma_x h_k \sigma_x = h_{-k}$

$$d_k^x = d_{-k}^x \quad (81)$$

$$d_k^y = -d_{-k}^y \quad (82)$$

$$d_k^z = -d_{-k}^z \quad (83)$$

$$\varepsilon_k = \varepsilon_{-k} \quad (84)$$

Therefore the combination of T and I imposes that $d_z(k) = 0$, as we wanted. This symmetry however does not impose that $\varepsilon_k = 0$, so in this sense, TI is a fine tuned symmetry. Often, ε_k does not enter the topological properties of the system, but one should be ware!

We can already observe some differences between these two choices. Although both of these symmetries (\hat{S} and $\hat{T}\hat{I}$) lead to the same conclusion, the constraint that $d_k^z = 0$, as we will see they have different physically observable consequences. \hat{S} protects a strong topological phase while $\hat{T}\hat{I}$ is an example of a crystalline topological phase because the former is a local symmetry while inversion is a spatial symmetry which is highly non-local (maps $x \rightarrow -x$).

To sum up, by our previous discussion we have two different gapped Hamiltonians if $d_k^z = 0$: one that encloses the origin as we change k and the other one that does not. What are the physical differences? As we anticipated in the introduction, topological phases have quantized observables in units of fundamental constants. Now we are going to see that these two types of insulators have a different quantized response, in this case the polarization. Lets define it.

B. Polarization, Berry phase and Zak phase

Spatially separated charges create a polarization. Loosely speaking, polarization is therefore related to the position operator (see Ref. [15] for an in-depth introduction)

$$P \sim \langle x \rangle \sim \langle i\partial_k \rangle.$$

Quantum mechanically the total polarization P is the sum over the polarization of all occupied bands $P = \sum_{n \in \text{occ}} P_n$. Given the intuition of (IV B) it is not surprising that the polarization for each occupied band n is defined as

$$P_n = -\frac{e}{2\pi} \int_0^{2\pi} dk \langle u_k^n | i\partial_k | u_k^n \rangle \equiv \frac{e}{2\pi} \Phi_n, \quad (85)$$

where n specifies the occupied band index with corresponding eigenvector $|u_k^n\rangle$. We have also defined Φ_n , known as the Zak phase of band n . The Zak phase is a particular instance of what we call a Berry phase:

$$\gamma_{\mathcal{C}} = \oint_{\mathcal{C}} \langle u_k^n | i\partial_k | u_k^n \rangle, \quad (86)$$

which is the integral of the Berry connection over a general closed path \mathcal{C} . The Zak phase corresponds to the particular choice where \mathcal{C} is a path traversing the Brillouin Zone, parametrized in this case by k as it goes from $k = 0$ to $k = 2\pi$.

Before discussing the polarization of the SSH model, let us discuss a few properties of P_n . First, the integrand of this expression appears so often that has its own name: the Berry connection.

$$A_k^n = i\langle u_k^n | \partial_k | u_k^n \rangle, \quad (87)$$

As you see it is defined for each band, and when we assign a different phase to the state vectors,

$$|u_k^n\rangle \rightarrow e^{-i\phi_k^n} |u_k^n\rangle, \quad (88)$$

then we see that the Berry connection transforms as

$$A_k^n \rightarrow A_k^n + \partial_k \phi_k^n, \quad (89)$$

This should remind you of the electromagnetic vector potential, which upon a gauge transformation changes as $\vec{A} \rightarrow \vec{A} + \vec{\partial}\phi$. You might also recall that in electromagnetism nothing should depend on the gauge we choose. In quantum mechanics, nothing should depend on the overall phase we choose either, so there is a parallelism here! Now if we apply (88) to our definition of polarization:

$$P_n \rightarrow -\frac{e}{2\pi} \left(\int_0^{2\pi} dk \langle u_k^n | i\partial_k | u_k^n \rangle + \int_0^{2\pi} dk \partial_k \phi_k^n \right) \quad (90)$$

$$= P_n + \frac{e}{2\pi} (\phi_{k=0}^n - \phi_{k=2\pi}^n) \quad (91)$$

Since a phase is defined up to an integer multiple of 2π we must have $(\phi_{k=0}^n - \phi_{k=2\pi}^n) = 2\pi m$ where m is an integer.

Thus the Berry phase (86) is defined up to integers of 2π and the polarization is only defined (modulo) e !

$$P_n = e \frac{\Phi_n}{2\pi} \bmod(e),$$

This is a striking result, first obtained by D. Vanderbilt [15]. However, this is not a problem. You might recall that only changes in polarization are actually measurable because they are gauge independent quantities. Imagine I want to calculate the change in polarization upon varying a given parameter λ . If we think of λ as time the derivative of P with respect to λ would be the current, i.e. the pumped charge in a time interval. The change in polarization along a path is given by

$$\Delta P_n(\lambda_i \rightarrow \lambda_f) = \int_{\lambda_i}^{\lambda_f} d\lambda \frac{dP_n}{d\lambda} \quad (92)$$

$$= -\frac{e}{2\pi} \int_{\lambda_i}^{\lambda_f} d\lambda \int dk \partial_\lambda A_k^n \quad (93)$$

$$\equiv -\frac{e}{2\pi} \int_S dS \Omega_{\lambda k}^n \quad (94)$$

Lets stop a moment. Here we have written the change in polarization as a flux over a quantity, which we call the Berry curvature of band n , defined as $\Omega_{xy}^n = \partial_x A_y^n - \partial_y A_x^n = -2\text{Im}\langle \partial_x u^n | \partial_y u^n \rangle$, which thus looks a lot like a magnetic field. For us the parameters that define the surface are λ, k and thus we have $\Omega_{\lambda k}^n = -2\text{Im}\langle \partial_\lambda u_k^n(\lambda) | \partial_k u_k^n(\lambda) \rangle$. What is interesting is that if the surface S is closed:

$$\oint_S dS \Omega_{\lambda k}^n = 2\pi C_n \quad (95)$$

with C_n an integer called the Chern number. The last equality follows from Chern's Theorem: the integral of the Berry curvature over a closed 2D surface is quantized [15]. We will encounter (95) later on when we discuss Chern insulators.

A last technical remark here: You might be wondering why is C_n not ambiguous, as happened with the Berry phase (86). It turns out that this is related to a condition in Stokes' theorem: if you demand that your gauge choice for ϕ_k is smooth and continuous over the whole surface S the result is guaranteed to be gauge invariant. However, for the path \mathcal{C} in (86) we have many such gauge choices, that leave an ambiguity of 2π .

1. Quantized polarization as a topological invariant for the SSH model

Now we are ready to calculate the Polarization on the two phases of the SSH model, $\delta > 0$ and $\delta < 0$. An easy limit is $\delta = 1$, where the eigenvectors are defined as

$$|u_k^{1,2}\rangle = \frac{1}{\sqrt{2}} \begin{pmatrix} \mp e^{ik} \\ 1 \end{pmatrix}$$

and we have $E_k = \pm 1$. If we carry out the differentiation and integration in Eq. (85), then we obtain

$$P = \frac{e}{2} \bmod(e). \quad (96)$$

However, if we choose $\delta = -1$, we see that

$$|u_k^{1,2}\rangle = \frac{1}{\sqrt{2}} \begin{pmatrix} \mp 1 \\ 1 \end{pmatrix}$$

with $E_k = \pm 1$ leading to

$$P = 0 \bmod(e). \quad (97)$$

Is this coincidence? No! In fact, you we now check that so long as $\delta > 0$ $P = \frac{e}{2}$, while if $\delta < 0$ $P = 0$, modulo e . To show this recall that the SSH Hamiltonian (71) is off diagonal (only depends on $\sigma_{x,y}$). Its off diagonal component can be written as $d_x + id_y = |\vec{d}|e^{i\phi_k}$ provided $|\vec{d}| \neq 0$ for all k , which is guaranteed in the gapped phase. In this case you can show that the eigenvectors can be written as

$$|u_k^\pm\rangle = \frac{1}{\sqrt{2}} \begin{pmatrix} \mp e^{i\phi_k} \\ 1 \end{pmatrix}$$

If we carry out the differentiation and integration in Eq. (85), then we obtain for the lower band

$$P = \frac{e}{2\pi} \int_{BZ} dk \frac{1}{2} \frac{\partial \phi_k}{\partial k} = m \frac{e}{2} \bmod(e) \quad (98)$$

The last equality follows from the fact that $\phi_k = \phi_{k+G}$ modulo an integer m times 2π , with G a lattice vector. Since this integer cannot be changed unless $|\vec{d}| = 0$ at some k , the polarization stays pinned to $e/2$ when $\delta > 0$ ($m = 1$) and to 0 when $\delta < 0$ ($m = 0$). See Ref. [16] for a pedagogical discussion.

P in the SSH model is an example of a quantized response: Polarization only depends on fundamental constants times a half quantized integer or zero. It also suggests that these two cases can be classified by a \mathbb{Z}_2 integer which takes the values one or zero depending on whether $P = \frac{e}{2}$ or $P = 0$. We can take this integer to be exactly $\Phi_n/2\pi$. This acts as a topological invariant, because, so long as the symmetries ensuring $d_z = 0$ are met, one cannot change continuously (i.e. without closing the gap) between the two types of insulators.

However, this is not the whole story. Another way to see that P is quantized is realizing that Φ_n is in fact $1/2$ of the solid angle swept by $\hat{d} = \vec{d}_k/|\vec{d}_k|$ as we change k from 0 to 2π (if this is not clear to you, this might be more evident in the next section, or you can convince yourself by direct computation). Since $d_z = 0$ because of chiral symmetry, \hat{d}_k is confined to the (\hat{d}_x, \hat{d}_y) plane. For $\delta < 0$ \hat{d}_k does not trace any solid angle, leading to $\Phi_n = 0$ and hence $P = 0$. For $\delta > 0$ it winds around the origin once, leading to a solid angle of 2π , which implies $\Phi_n = \pi$ and $P = e/2$. This suggests that \hat{d} can wind more than once, which means we can classify distinct topological phases with an integer \mathbb{Z} : the winding number of d_k around the origin. Indeed, any single-particle Hamiltonian with chiral symmetry can be written as

$$h(k) = \begin{pmatrix} 0 & q_k \\ q_k^\dagger & 0 \end{pmatrix}, \quad (99)$$

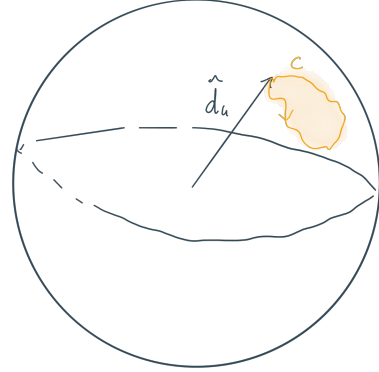


Figure 5. The Berry phase of two-band models is half the solid angle swept by $\hat{d} = \vec{d}_k/|\vec{d}_k|$. For the SSH chain \hat{d} is confined to the plane, and the solid angle is either zero or 2π , leading to a Berry phase of 0 or π .

for which we can define a winding number [17]

$$\nu = \frac{i}{2\pi} \int_k \text{Tr}[q_k \partial_k q_k^\dagger] \in \mathbb{Z} \quad (100)$$

which counts how many times \vec{d}_k winds around the origin (i.e. how many times \vec{d}_k intersects a line from the origin to infinity). It relates to the polarization as

$$P = e \frac{\nu}{2} \bmod(e). \quad (101)$$

To see what is the physical differences between different ν we need to look at a different observable: the number of edge states.

C. The invariant from inversion eigenvalues

You might have noticed that in the Brillouin zone there are special momenta that satisfy $k = -k$ modulo a lattice vector: these are $k = 0, \pi$. We may call these inversion symmetric momenta, because inversion takes $k \rightarrow -k$. This is true independent of the system we are considering.

Lets take a look at the SSH Hamiltonian at these special points. The Hamiltonian reads

$$h_k^{\alpha\beta} = \vec{d}_k \cdot \vec{\sigma} + \varepsilon_k \sigma_0 \quad (102)$$

where we $\varepsilon_k = 0$ and

$$\vec{d}_k = ((1 - \delta) + (1 + \delta) \cos k, (1 + \delta) \sin k, 0). \quad (103)$$

Hence $h_{k=0} = ((1 - \delta) + (1 + \delta))\sigma_x = 2\sigma_x$ and $h_{k=\pi} = -2\delta\sigma_x$. We immediately notice that the gap closes at $k = \pi$ when $\delta = 0$ while it remains open at $k = 0$ for all δ . It turns out, that we can use this information to track the change

of the topological phase, and define a topological invariant, much more easily than before. To do so we must track the band closing, and a way to do this is by symmetry labeling the bands.

First, recall that for our SSH Hamiltonian, inversion was represented by σ_x . In other words our SSH Hamiltonian satisfies $\sigma_x h_k \sigma_x = h_{-k}$. Observe that there are two special momenta that under inversion are mapped to themselves, $k = 0, \pi$, up to a reciprocal lattice vector. At these points, the Hamiltonian commutes with inversion, which means we can label the bands with inversion eigenvalues. Let's see how that happens. Where this is a symmetry that commutes with

The Hamiltonian at $k = 0, \pi$ is very simple:

$$h_{k=0} = 2\sigma_x, \quad h_{k=\pi} = -2\delta\sigma_x \quad (104)$$

which have eigenvalues ± 2 and $\mp 2\delta$ respectively. At half-filling (one electron per site) only the lowest eigenvalue is filled for each momentum point. Now we ask, what are the inversion eigenvalues of the filled bands. For h_0 , the eigenvalues are independent of δ , and the filled state is always the same: that with eigenvalue -2 and eigenvector $\frac{1}{\sqrt{2}}(-1, 1)$. Now this state is an eigenvector of the inversion operator with eigenvalue $\xi_{k=0} = +1$, as shown in Fig. 6 (in this example, this is simple to see because both the Hamiltonian and inversion are represented by σ_x). The situation is different at $k = \pi$. If $\delta < 0$ the filled state is $\frac{1}{\sqrt{2}}(-1, 1)$ with inversion eigenvalue $\xi_{k=\pi} = +1$ but for $\delta > 0$ the filled state is $\frac{1}{\sqrt{2}}(1, 1)$ with eigenvalue $\xi_{k=\pi} = -1$. Note that the product $\xi_{k=0}\xi_{k=\pi}$ therefore only changes when the gap closes, at $\delta = 0$. Therefore we can use symmetry to indicate the topological state of our chain by defining:

$$\nu_{\mathbb{Z}_2} \equiv \xi_{k=0}\xi_{k=\pi} = \pm 1 \quad (105)$$

The two cases ± 1 are not connected to each other unless we cross a gapless point (see Fig. 6).

Note as well that this invariant can be viewed as the answer to the question: is the solid angle traced by \hat{d} equal to 0 or 2π . A value $\nu_{\mathbb{Z}_2} = -1$ indicates that \hat{d} points along \hat{x} when $k = 0$ and along $-\hat{x}$ when $k = \pi$. This means that as k is varied from 0 to 2π , \hat{d} traces an arc that spans 2π radians from the origin.

$\nu_{\mathbb{Z}_2}$ is the first example of a topological invariant constructed using symmetry indicators: using a unitary symmetry of our system, we can determine whether or not the system is in a topological state. This statement turns out to be quite general: spatial symmetries simplify the calculation of topological invariants. The eigenvalues $\xi_{k=0, \pi}$ that compose expressions like (128) are known as symmetry indicators of band topology, or simply symmetry indicators. Note that calculating the invariant in this way we can only distinguish between two values ± 1 , and thus it is a \mathbb{Z}_2 invariant. Sometimes using symmetry is enough to say which state is topological, but it is not enough to teach us about the full classification of this state (\mathbb{Z} vs \mathbb{Z}_2 in the SSH case). This can happen in higher dimensions: e.g. the Chern number of 2D models, an invariant we will introduce soon, can be calculated modulo an integer using spatial symmetries, but in general it takes any integer value.

D. Edge States

While the imposition of certain symmetries is enough to guarantee this quantized behavior, the presence (or absence) of edge states depends on whether the type of symmetry that protects the topological phase is spatial or not. First, let's gather some properties of the chiral symmetry in the SSH model that we have seen:

- ε_k breaks chiral symmetry ($Uh_k U_S^\dagger \neq -h_k$) which, for the SSH chain takes the form $U_S = \sigma_z$.
- U_S is local in space (does not depend on the site).
- For every state with energy ε we have another state at energy $-\varepsilon$.

Imagine we have a finite SSH chain and we consider the two limits $\delta = 1$ and $\delta = -1$ as in Fig. 7. Since we don't have periodicity, the spectrum cannot be represented as a function of momentum k , but we can still plot it as shown in Fig. 8. For a finite chain, the only difference between $\delta = 1$ and $\delta = -1$, is that for the former case $c_{A,i}$ and $c_{B,L}$ are not connected to any site by any term in the Hamiltonian. This is equivalent to saying that the Hamiltonian has two rows of zeros, which implies that there are two $E = 0$ eigenvalues when $\delta = 1$. These edge states are absent when $\delta = -1$, because the connectivity of the lattice is different. The presence of edge states is in fact not a coincidence of our choice of parameters, but rather a consequence of chiral symmetry, locality of the Hamiltonian and that $\delta > 0$ combined. Let's see why.

Imagine we want to lift the degeneracy of the edge states that occur at $\delta = 1$. First, we notice that the bulk gap closes at $\delta = 0$. Since we want to ask if the edge states are a topologically protected property of the gapped phase, we are not allowed to cross $\delta = 0$, and thus we are restricted to $\delta > 0$.

Perhaps, you think, we can keep $\delta > 0$ but lift the degeneracy moving away from $\delta = 1$, which is a suspiciously special parameter choice. However, moving away from $\delta = 1$ cannot lift the degeneracy at zero. The reason is best understood if we consider first a semi-infinite chain. In a semi-infinite chain we have only one edge state. This localized edge state, is an eigenstate of chiral symmetry ($U_S = \sigma_z$); all eigenstates are. Now recall that eigenvalues come in $(-E, E)$ pairs, and that these pairs are related by chiral symmetry. If we only have one localized state, we must have it at $E = 0$. If we only have one, no perturbation that respects chiral symmetry can lift it from zero, because this will imply we have a state at $\pm E$ without a partner at $\mp E$. Moving back to a finite chain, our arguments are independently true for both end states, so, even if we move from $\delta = 1$, the two end-states will remain at zero (they are chiral partners).

Aha! you say, but we can move one edge state up in energy, say to E , and one down in energy $-E$, so that they form a $(-E, E)$ pair! Indeed, this is possible, but here is where the locality requirement enters: to do this we need to add a term $c_{A,1}^\dagger c_{B,N} + \text{h.c.}$ that couples the two end states. However, this would be a non-local term and would violate our locality principle: hopping terms must be local (i.e. short range).

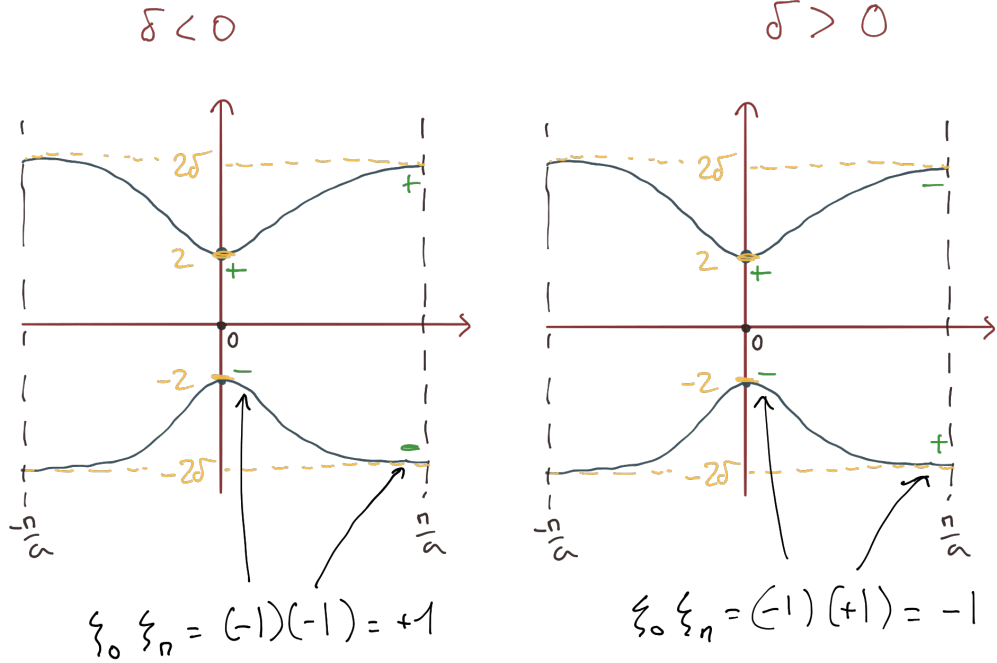


Figure 6. The trivial (left) and topological (right) can be distinguished by the product of inversion eigenvalues of filled bands at the two inversion invariant points $k = 0, \pi$.

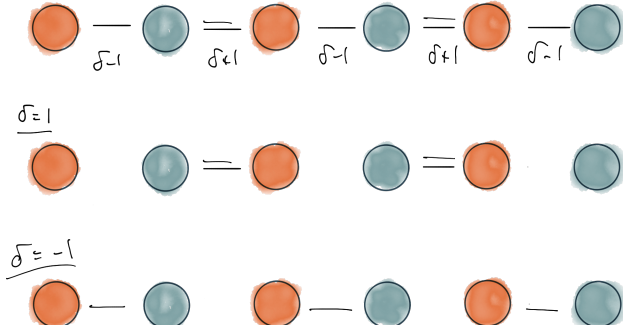


Figure 7. There are two easy limits where to see the emergence of absence of edge states $\delta = 1$ and $\delta = -1$.

Lastly, we could also try a term like $c_{A,1}^\dagger c_{A,1}$ or $c_{B,1}^\dagger c_{B,1}$, which is an onsite term and it is local. However, this term will break chiral symmetry because it will enter like σ_0 or σ_z , spoiling the condition $U h_k U_S^\dagger \neq -h_k$ with $U_S = \sigma_z$.

We must conclude that, as long as we do not close the gap between the bulk states, there is no way to break the degeneracy

of the edge states without breaking the chiral symmetry that protects the state. Moreover, we notice that even if we add copies of the chain (say \mathbb{Z} copies), so long as only have A to B terms chiral symmetry will be respected, and we will have \mathbb{Z} copies of the edge state. This is what the index ν in (100) counts.

One final note: What would have happened if we had used the combination of time-reversal and inversion to protect the topological phase? Inversion sends $x \rightarrow -x$ so $P \rightarrow -P$. Since P is defined only modulo e , if we have inversion symmetry there are two values that satisfy $P = -P$, which are $P = 0, \frac{e}{2}$, which correspond to Zak phases of $\Phi = 0, \pi$, respectively. Based on polarization we could distinguish two type of insulators, with a \mathbb{Z}_2 number: $\Phi/2\pi$. It is possible to show that chiral symmetry also suffices to quantize $P = 0, \frac{e}{2}$. However, while chiral symmetry protects the edge states to be at zero energy, safe from the bulk states, inversion and time-reversal cannot protect zero energy edge states. To see this note that we could have added a term $\mu(c_{A,1}^\dagger c_{A,1} + c_{B,1}^\dagger c_{B,1})$ corresponding to a term $\mu\sigma_0$ in the Hamiltonian. This term respects inversion symmetry, in virtue of 84. However, as we saw before, this term can move the zero energy states away from zero energy, and thus this crystal symmetry is not enough to protect the edge states.

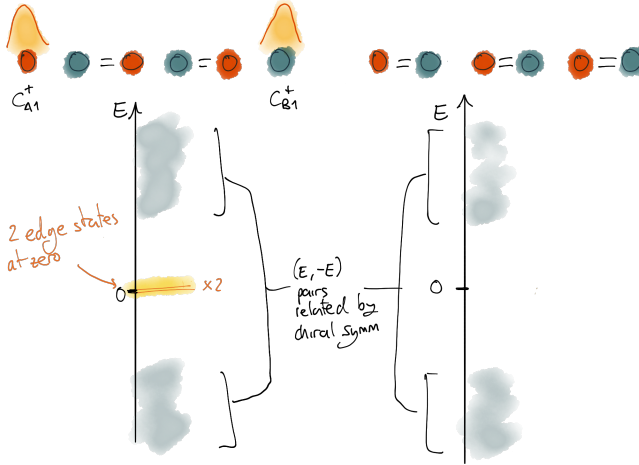


Figure 8. The left figure shows that in the case where $\delta = 1$, $c_{A,1}^\dagger$ and $c_{B,N}^\dagger$ drop from the Hamiltonian. Therefore it costs zero energy to create states at the edges. These are cannot be removed by any local perturbation that preserves chiral symmetry.

E. Edge states from the Dirac equation

A very convenient way to analyze topological phase transitions and make analytical progress is to expand the tight-binding Hamiltonian around relevant k points. We have already seen that compared to $k = 0$, $k = \pi$ is a very special point, where the gap closes if $\delta = 0$. This is also verified if we expand the Hamiltonian to linear order in k :

$$h_{k \sim 0} \approx tk\sigma_y + 2t\sigma_x \quad (106)$$

$$h_{k \sim \pi} \approx -tk\sigma_y - 2t\delta\sigma_x \quad (107)$$

The fact that the gap closes at $\delta = 0$ is captured in the linear approximation. Now, we know that $\delta > 0$ and $\delta < 0$ should be also different. Thus, if we create a boundary between the two systems, where $\delta > 0$ for $x > 0$ and $\delta < 0$ for $x < 0$ we should be able to recover that there is a zero mode at the boundary. We focus on $h_{k \sim \pi}$ because, unlike $h_{k \sim 0}$, it depends on δ , and write it in a slightly different notation:

$$h_{k \sim \pi} \approx k\sigma_y + m\sigma_x \quad (108)$$

Hamiltonians that are linear in momentum written in terms of Pauli matrices are called Dirac Hamiltonians (We will use them in other dimensions too, e.g. in 2D they take the form $(h_k = k_x\sigma_x + k_y\sigma_y + m\sigma_z)$). The last term, where we have defined $m \equiv -2\delta$, sets the gap. It is usually called a mass term because the dispersion relation is

$$h_{k \sim \pi} \approx \pm \sqrt{k^2 + m^2} \quad (109)$$

which is like a relativistic particle with mass m .

Jackiw and Rebbi found out that if we allow m to change sign as a function of position, it must host a zero mode [18]. Lets show this by choosing any profile, $m(x)$ that satisfies $m(\pm\infty) = \pm m$. In our tight-binding language this amounts to demanding that the hoppings are inverted at some point (lets

fix that to $x = 0$), that we call the boundary, between a chain with $\delta > 0$ and a chain with $\delta < 0$. Now somewhere in the middle $\delta = 0$ but can we find a $E = 0$ solution? To answer this we must first write (108) in real space by using $k \rightarrow -i\partial_x$ and solve the following Schrodinger equation:

$$\begin{pmatrix} 0 & -i(-i\partial_x) + m(x) \\ +i(-i\partial_x) + m(x) & 0 \end{pmatrix} \psi = 0 \quad (110)$$

and find a normalizable $\psi = (\psi_+, \psi_-)$, a two component wave-function. This amounts to solving $\mp\partial_x\psi_\mp + m(x)\psi_\mp = 0$. There is only one normalizable solution:

$$\psi = \frac{1}{\mathcal{N}} e^{-\int_0^x dx' m(x')} \begin{pmatrix} 1 \\ 0 \end{pmatrix} \quad (111)$$

because a solution with $(0, 1)$ comes with a plus sign in the exponential and thus grows exponentially away from the boundary. A typical choice of mass profile to see the localized mode is $m(x) = m \tanh(x/\lambda)$ which interpolates between $m(\pm\infty) = \pm m$ by changing around the origin over a characteristic distance λ . The exponential factor leads to a localized mode with energy $E = 0$, just as we found previously. Additionally, note that the Dirac Hamiltonian (108) has chiral symmetry ($U_S = \sigma_z$) and thus this mode cannot move from zero energy unless chiral symmetry is broken.

The low-energy, or $k \cdot p$ Hamiltonians are a very useful tool to understand the emergence of edge states and topological properties analytically in all dimensions. We will keep this in mind when we introduce Chern insulators and topological insulators.

F. Wannier centers and charge pumping

To close the discussion of physical properties of the SSH model and introduce and use the Rice-Mele model we will discuss what is known as a Thouless pump.

The notion of Thouless pump can be understood by introducing a physical interpretation of the Zak phase: it tells us where the center of charge (known as Wannier center) is located in the unit cell. The Wannier center is the inverse Fourier transform of the Bloch function $\psi_{n\mathbf{k}}(\mathbf{r}) = e^{i\mathbf{k} \cdot \mathbf{r}} u_{n\mathbf{k}}(\mathbf{r})$, where $u_{n\mathbf{k}}(\mathbf{r})$ is the cell periodic function.

$$|w_{n\mathbf{R}}\rangle = \frac{V_{cell}}{2\pi} \int_{BZ} e^{i\mathbf{k} \cdot \mathbf{R}} |\psi_{n\mathbf{k}}\rangle \quad (112)$$

The nice thing about wannier functions $|w_{n\mathbf{R}}\rangle$ is that as long as $\psi_{n\mathbf{k}}(\mathbf{r})$ is a smooth function of \mathbf{k} then $w_{n\mathbf{R}}(\mathbf{r})$ decays rapidly with \mathbf{R} . In fact they are localized near \mathbf{R} [15] so it decays fast with $|\mathbf{r} - \mathbf{R}|$. The center of charge of the Wannier function is given by the diagonal element:

$$\bar{r}_n = \langle w_{n0} | \hat{\mathbf{r}} | w_{n0} \rangle \quad (113)$$

It is not difficult to show (see Chapter 3, eq. 3.96 in Vanderbilt's book [15]) that

$$\bar{r}_n = \frac{V_{cell}}{2\pi} \int_{BZ} \langle u_{n\mathbf{k}} | i\partial_{\mathbf{k}} | u_{n\mathbf{k}} \rangle \quad (114)$$

In 1D, this is exactly given by the Zak phase!

$$\bar{x}_n = a \frac{\Phi_n}{2\pi} \quad (115)$$

where n labels the band (to know the position of the Wannier center in the crystal we would add an integer X_i that labels the the unit cell), and we have restored the lattice constant a .

Now recall that because of inversion symmetry $\Phi_n = 0, \pi$. This, in the position operator language means that the charge center of band n is situated either on top of a site, or in the middle of the bond. This makes sense, because these are the only two inversion symmetric points in the unit cell! It also tells us that the difference between these two situations is half a lattice spacing $\Delta x = a/2$, in other words a change in polarization $\Delta P = \frac{e}{a} \Delta x = \frac{e}{2}$.

We are ready to define a Thouless pump which is a closed path interpolating between these two situations. Since we now know that in the presence of inversion symmetry the charge center can only be either on top of a site or in the middle of the bond, we need to break inversion symmetry to move it. This is precisely what the Rice-Mele model parameter Δ does. Recall that the Rice-Mele Hamiltonian is given by (see our discussion close to Eq. 21)

$$H = \mathbf{d}_k \cdot \vec{\sigma} + \varepsilon_k \cdot \mathbb{1} \quad (116)$$

where

$$\mathbf{d}_k = (t(1 - \delta) + t(1 + \delta) \cos k, t(1 + \delta) \sin k, m). \quad (117)$$

The term Δ breaks inversion; you can check this mathematically using (68) and $\hat{I} = \sigma_z$. Physically this is because the onsite staggered potential m adds an onsite energy of $+\Delta$ to sites A and $-\Delta$ to B sites, and thus we don't recover the same change upon exchanging A and B sites.

Now imagine we consider a closed path in the parameter space set by the two free parameters of our model (δ, Δ) , see Fig. 9. Let's assume that we start at $(\lambda, \Delta) = (-1, 0)$ with $P = 0$ and $\Phi_z = 0$, which then dictates that we place the Wannier center of charge on a site, which is an inversion symmetric point. As we cycle through values of the parameter (λ, Δ) , the charge distribution translates through the unit cell. When $(\lambda, \Delta) = (1, 0)$, the charge is located at the center of the unit cell, but when $\Phi_z = \pi$, the charge is located at the edge of the unit cell. Running through this cycle pumps exactly a charge across each unit cell in the system. If we parametrize the path by an angle ϕ the change in polarization is given by Eq. 92

$$\Delta P = -\frac{e}{2\pi} \int_0^{2\pi} d\phi \int_0^{2\pi/a} dk \Omega_{\phi k}. \quad (118)$$

Since our path is periodic, the surface of integration is closed. Hence by (95) we get an integer, $C_n = 1$ times e .

Although the Thouless pump was predicted long ago [19], it has only been observed recently in systems of ultra-cold atoms [20, 21].

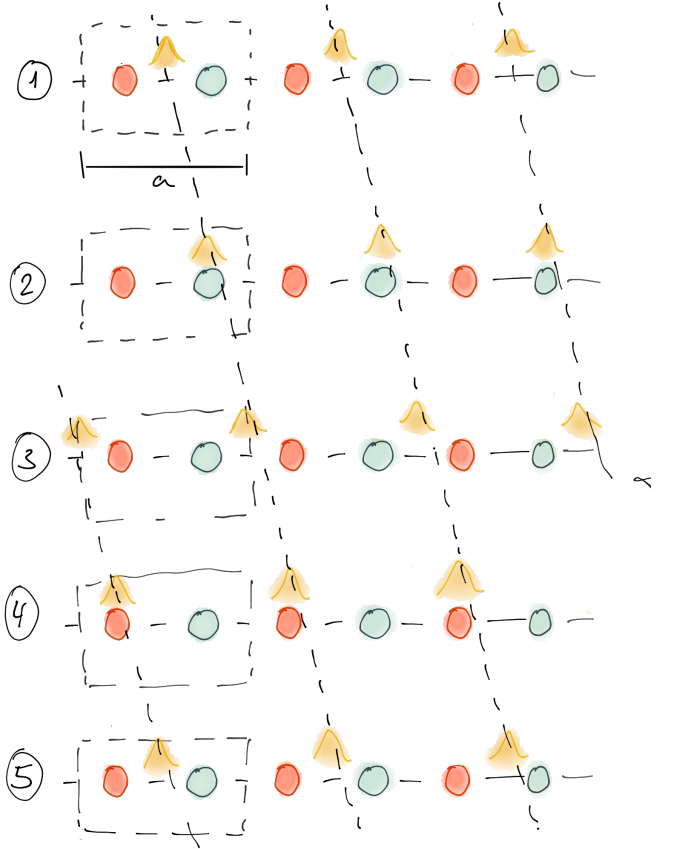
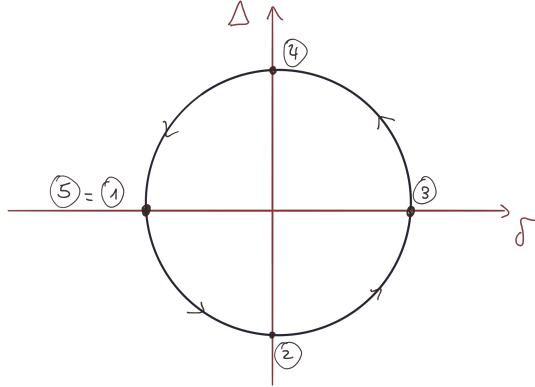


Figure 9. Thouless pump exemplified by a closed loop in (λ, Δ) . The difference between 1 and 3 is a displacement of $e/2$ while from 1 to 5 we have pumped exactly one charge through the unit cell.

G. The SSH model and the 10-fold way

We have seen that if the SSH has chiral symmetry is classified by a \mathbb{Z} invariant. When we have a topological phase protected by a non-unitary symmetry we call it a strong topological phase. When can a model be in a strong topological phase? The possibilities depend on which non-unitary sym-

metries this model has, and the topological invariants one can build. All the possibilities are tabulated in [V](#).

We see that the chiral SSH model belongs to class AIII if it lacks time-reversal and particle hole symmetries but it is in class BDI if it satisfies these symmetries and $T^2 = 1$. The example we considered was in class BDI. To see this recall that our electrons were spinless. Thus $T^2 = 1$ and T can be chosen to be simply complex conjugation. Therefore \hat{T} was a symmetry because $U_T h_{-k}^* U_T = h_k$ with U_T the identity.

Similarly, we will see that in other dimensions other topological phases exist for different non-unitary symmetries. We will focus on the examples of a Chern insulator, and a 3D Topological insulator

H. 1D insulators are obstructed insulators

What we have learned from the above is that topological insulators have edge states, and quantized responses. However we have been able to understand all the phenomenology in terms of Wannier states, which are exponentially localized. As depicted in [Fig. 9](#), we can interpolate between an atomic insulator, where the charge centers sit at the sites, and an insulator where the charge centers sit at the bonds. For this reason, sometimes it is said that in 1D there are no true topological insulators: all insulators are connected to atomic limits. However, symmetry plays a crucial role: if we respect inversion symmetry (inversion imposes $\Delta = 0$), the two insulators cannot be connected unless we close the gap. Since there is a symmetry obstruction to connect these two insulators, 1D topological models are sometimes called obstructed insulators.

This contrasts what happens in higher-dimensions. We could define topological phases as those that do not have atomic limits. In fact, it is possible to show [\[15\]](#) that if you try to find a localized Wannier basis to describe a topological phase, you run into problems. The reason is that you cannot normalize the states because their normalization, set by the overlap of Wannier like functions, is guaranteed to be singular at some k point [\[15\]](#).

I. Example II: Kitaev Wire

One might worry that the SSH chain is not very robust to perturbations. For example, any hopping that couples A atoms to A atoms (or B to B), like second-nearest neighbours will break chiral symmetry (introduce a term with σ_z or ε_k).

A more robust phase in 1D is a topological 1D superconductor protected by particle-hole symmetry. As we saw in section [III B 3](#) BdG Hamiltonians have exact chiral symmetry. This symmetry can be used to protect topological phases in 1D.

Kitaev proposed a model to realize this phase with spinless electrons hopping on a 1D lattice, like in [Eq. \(5\)](#), but with a nearest neighbour pairing term Δ

$$H = -\mu \sum_i^L \hat{n}_i - \frac{1}{2} \sum_i^L (t \hat{c}_i^\dagger \hat{c}_{i+1} + \Delta c_i c_{i+1} + \text{h.c.}) \quad (119)$$

Imposing periodic boundary conditions and going to k space we can use the recipe of [Sec. III B 3](#) to construct our BdG hamiltonian:

$$H = \frac{1}{2} \sum_k \chi_k^\dagger h_k^{\text{BdG}} \chi_k \quad (120)$$

with $\chi_k^\dagger = (c_k^\dagger, c_{-k})$ and

$$h_k^{\text{BdG}} = \begin{pmatrix} \epsilon_k & \tilde{\Delta}_k^* \\ \tilde{\Delta}_k^* & -\epsilon_k \end{pmatrix} \quad (121)$$

with $\epsilon_k = -t \cos(ka) - \mu$ and $\tilde{\Delta}_k = -i\Delta \sin(ka)$. Note that pairing Δ can be complex in general $\Delta = |\Delta|e^{i\phi}$, but we will not worry about this too much. Also, sometimes a pairing like $\tilde{\Delta}_k$ is called *p*-wave pairing, reflecting the fact that at small momenta the pairing term goes as k and is thus an odd function of momentum. k -independent pairings are called *s*-wave pairing. This Hamiltonian looks a lot like the SSH model with a different choice of matrices. We can write it as usual for 2×2 hamiltonians:

$$h_k^{\text{BdG}} = \vec{d}_k^{\text{BdG}} \cdot \vec{\tau} + \varepsilon_k \tau_0 \quad (122)$$

with

$$\vec{d}_k^{\text{BdG}} = (0, -\Delta \sin(ka), -t \cos(ka) - \mu) \quad (123)$$

and $\varepsilon_k = 0$. We have used the Pauli matrices $\vec{\tau}$ instead of $\vec{\sigma}$ to remind us that the 2×2 structure of the Hamiltonian is not physically a spin, but rather electrons and holes.

The bands are given simply by $E^\pm = \sqrt{\epsilon_k^2 + |\tilde{\Delta}_k|^2}$. By plotting the bands you can see that the bands have a gap, except for $\mu = \pm t$.

As we learned in [Sec. III B 3](#) the Nambu spinor χ is not independent of χ . In k -space this translates to $(\chi_{-k}^\dagger)^t = \tau_z \chi_k$ which imposes particle-hole symmetry: $U_C h_k^* U_C^\dagger = -h_{-k}$ which imposes:

$$d_k^x = -d_{-k}^x \quad (124)$$

$$d_k^y = -d_{-k}^y \quad (125)$$

$$d_k^z = d_{-k}^z \quad (126)$$

$$\varepsilon_k = -\varepsilon_{-k} \quad (127)$$

which is indeed satisfied by [\(122\)](#). In the absence of any other symmetry this model belongs to Class D of [Table V](#). Since we are in $d = 1$ We can read from the table it has a \mathbb{Z}_2 invariant which we know how to calculate!

Assume that $|\vec{d}_k^{\text{BdG}}| \neq 0$, which is equivalent to assuming that the bands have a gap. Then one can define again $\hat{d}_k = \vec{d}_k^{\text{BdG}} / |\vec{d}_k^{\text{BdG}}|$ and check its winding number. From our discussion in the SSH we can again check how this vector changes as we move the momentum in from 0 to 2π . We notice inversion is represented by τ_z and the same discussion leads us to define its eigenvalues at the inversion symmetric points

$$\nu_{\mathbb{Z}_2} \equiv \xi_{k=0} \xi_{k=\pi} = \pm 1 \quad (128)$$

Class	\hat{T}	\hat{C}	\hat{S}	$d = 1$	$d = 2$	$d = 3$
A	0	0	0	0	\mathbb{Z} (e.g. CI)	0
AIII	0	0	1	\mathbb{Z}	0	\mathbb{Z}
AI	1	0	0	0	0	0
BDI	1	1	1	\mathbb{Z} (e.g. SSH)	0	0
D	0	1	0	\mathbb{Z}_2 (e.g. Maj. wire)	\mathbb{Z}	0
DIII	-1	1	1	\mathbb{Z}_2	\mathbb{Z}_2	\mathbb{Z}
AII	-1	0	0	0	\mathbb{Z}_2 (e.g. 2DQSH)	\mathbb{Z}_2 (e.g. 3DTI)
CII	-1	-1	1	$2\mathbb{Z}$	0	\mathbb{Z}_2
C	0	-1	0	0	$2\mathbb{Z}$	0
CI	1	-1	1	0	0	$2\mathbb{Z}$

Table V. 10-fold classification of non-unitary symmetries with trivial and non-trivial classes in different dimensions.

Once again this invariant is telling us how the vector \hat{d}_k winds around the origin as we change k . For $k = 0$ it points at $-\text{sign}(t + \mu)\hat{z}$ while for $k = \pi$ it points at $\text{sign}(t - \mu)\hat{z}$. Hence the topological invariant is $\nu_{\mathbb{Z}_2} = -1$ only when $\mu < t$, which realizes the topological phase.

This topological phase also has edge states. They become apparent by changing fermionic creation and anihilation operators into majorana fermions ($\gamma_{\alpha,j}$)

$$c_j = \gamma_{B,j} + i\gamma_{A,j} \quad (129)$$

which need to satisfy:

$$\{\gamma_{\alpha,i}, \gamma_{\beta,j}\} = \delta_{\alpha\beta}\delta_{ij} \quad \gamma_{\alpha,j} = \gamma_{\alpha,j}^\dagger \quad (130)$$

As an exercise you can try to derive the Hamiltonian in terms of Majorana fermions, which looks a lot like the SSH Hamiltonian (see [22]). It follows that there are two unpaired Majoranas modes at zero energy in the topological phase.

There is a difference between the end modes in a Majorana Chain and an SSH chain. In the SSH there is an inherent ambiguity in the unit cell, and this can change the number of zero modes [23]. Since the two Majorana states are formed from one electron there is no such ambiguity in the Kitaev chain (see Ref. [24] for a thorough discussion).

A last remark. The fact that we started with spinless electrons is crucial for the stability of the phase. If you have spin, there will be two majorana endmodes at the end of the chain, which can form a fermion, and gap out (they will not necessarily be at zero energy). Getting read of this problem, known as fermion doubling is the reason why current attempts to isolate Majorana end modes in nano-wires are focused on large-spin orbit coupled materials with a magnetic field. Their effect combined creates an effective spinless Kitaev model. I might add something about this in future versions of the notes, but an excellent discussion is in the review by J. Alicea [22].

V. CHERN INSULATORS: TOPOLOGICAL PHASES IN 2D

A. Chern Insulators and the Chern number

Chern insulators are topological insulators in class A in $d = 2$. They are the only topological insulators in this symmetry class in physical dimensions ($d = 1, 2, 3$). In this class all

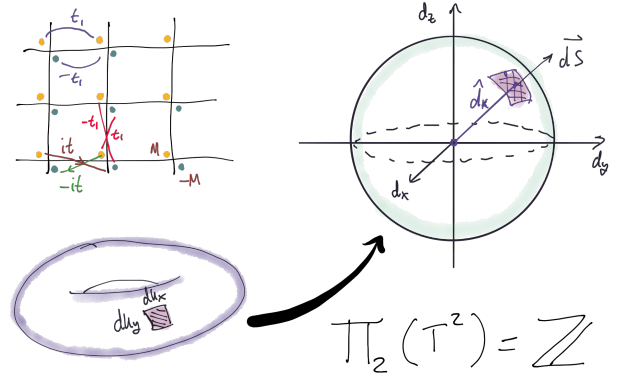


Figure 10. Top left: Chern insulator model in real space with the unit cell. The Brillouin zone is a torus, which maps the Hamiltonian into a unit two-sphere. The number of times the unit vector \hat{d}_k covers the unit sphere is the Chern number.

three anti-unitary symmetries are absent! and yet we can still define a \mathbb{Z} topological invariant. An easy example to see how this is possible is to again consider a generic two-band model in two dimensions. We can write:

$$h^k = \mathbf{d}_k \cdot \boldsymbol{\sigma} + \varepsilon_k \sigma_0 \quad (131)$$

$$E_k = \pm |\mathbf{d}_k| + \varepsilon_k. \quad (132)$$

But now $\mathbf{k} = (k_x, k_y)$. As before, $|\mathbf{d}_k| \neq 0$ is the condition that ensures a gap, and we ignore $\varepsilon_k = 0$, since it does not affect what comes next. We may again define a unit vector,

$$\hat{d}_k = \frac{\mathbf{d}_k}{|\mathbf{d}_k|}, \quad (133)$$

which lives on the surface of a sphere with radius 1, called S^2 , or the “two-sphere” (an n -sphere is designated S^n). On the other hand, the k -vector lives on the Brillouin Zone, which has the topology of a torus, $\mathbf{k} \in T^2$. The definition (133) defines

a map from the Brillouin Zone torus, to the two-sphere:

$$\mathbf{k} \rightarrow \hat{d}_{\mathbf{k}} \quad (134)$$

$$T^2 \rightarrow S^2. \quad (135)$$

We learned from our SSH example that the solid angle spanned by $\hat{d}_{\mathbf{k}}$ in the equator was a topological invariant. $\hat{d}_{\mathbf{k}}$ was constrained to the equator because we had chiral symmetry. Can we build an invariant even if we have no symmetry?

Lets try to find out what is the solid angle spanned by $\hat{d}_{\mathbf{k}}$ as we move \mathbf{k} in the Brillouin zone. Moving an infinitesimal amount in the k_x direction $\mathbf{k} \rightarrow \mathbf{k} + dk_x \hat{x}$ implies an infinitesimal change in $\hat{d}_{\mathbf{k}}$ given by $\hat{d}_{\mathbf{k}+dk_x \hat{x}} - \hat{d}_{\mathbf{k}} = \partial_{k_x} \hat{d}_{\mathbf{k}} dk_x$. Similarly for $\mathbf{k} \rightarrow \mathbf{k} + dk_y \hat{y}$ the change in $\hat{d}_{\mathbf{k}}$ is given by $\partial_{k_y} \hat{d}_{\mathbf{k}} dk_y$ (see Fig.(10)). The surface element of the two sphere perpendicular to the surface is then

$$d\mathbf{S} \equiv \partial_{k_x} \hat{d}_{\mathbf{k}} dk_x \times \partial_{k_y} \hat{d}_{\mathbf{k}} dk_y \quad (136)$$

Now we want to know how much of the sphere's surface is covered by moving in the Brillouin Zone. To this end we compute how much solid angle is swooped by $\hat{d}_{\mathbf{k}}$ [25]

$$C = \frac{1}{4\pi} \int \hat{d}_{\mathbf{k}} \cdot d\mathbf{S} \quad (137)$$

$$= \frac{1}{4\pi} \int dk_x dk_y \hat{d}_{\mathbf{k}} \cdot (\partial_{k_x} \hat{d}_{\mathbf{k}} \times \partial_{k_y} \hat{d}_{\mathbf{k}}) \quad (138)$$

with $C \in \mathbb{Z}$. The quantization is Chern's theorem, that we already discussed. One way to understand that you must have an integer is that otherwise we will be defining a bounded area on the surface of the sphere. In turn, this should correspond to some boundary on the torus, and there are no boundaries on the torus.

A note on nomenclature. The topological statement of this fact is $\Pi_2(T^2) = \mathbb{Z}$. This you can read that the the mapping from the torus to the two-sphere. The sub-index in Π , in this case 2, is the n -sphere to which we map whatever is inside the brackets. is characterized by an integer number. A more intuitive example is $\Pi_1(S^1) = \mathbb{Z}$. Here we are saying: the winding a circle with a circle is an integer. Similarly $\Pi_n(S^n) = \mathbb{Z}$. However, if we want to map a circle to a two-sphere $\Pi_1(S^2) = 0$. This intuitive because every circle on the top of the sphere can be topologically contracted to a point: all circles on the sphere are equivalent. In general $\Pi_n(S^m) = 0$ for $m > n$.

Thus far we have only considered a two band model. In this case the Chern number of the two bands are related: $C_1 = -C_2$. A Chern number can be defined for any isolated band, and is not only a property of two band models. We have already seen how to define it. Look at our definition of the change in polarization Eq. (92) and consider λ to be a momentum in a second direction. This immediately leads to the definition of the Chern number C_n for each band:

$$C_n = \frac{1}{2\pi} \int_{BZ} dk_x dk_y \Omega_{\mathbf{k}}^n \quad (139)$$

$$\Omega_{\mathbf{k}}^n = \vec{\nabla} \times \vec{A}_{\mathbf{k}}^n \quad (140)$$

$$\mathbf{A}_{\mathbf{k}}^n = i \langle u_{\mathbf{k}}^n | \tilde{\nabla}_{\mathbf{k}} | u_{\mathbf{k}}^n \rangle, \quad (141)$$

We see that the Chern number is the flux of the Berry curvature, which is the curl of the Berry connection. By analogy with Eq. (92) it is the quantized change in Polarization as we move in momentum space.

Chern numbers are defined in two spatial dimensions (or for cuts of higher-dimensional Brillouin Zones as we will see later on). Lets collect some useful properties of C_n :

1. Each isolated band in 2D has a Chern number, C^n .
2. Time-reversal symmetry implies that $C^n = 0$ for all bands n . This is because time-reversal symmetry implies that $\Omega_{\mathbf{k}} = -\Omega_{-\mathbf{k}}$. The Berry curvature integrated over a periodic region (the Brillouin-Zone) yields zero. This can be understood physically by remembering that $\mathbf{A}_{\mathbf{k}}^n$ determines the polarization, which is time-reversal symmetric, but $\Omega_{\mathbf{k}}$ has an extra derivative of momentum.
3. Inversion requires $\Omega_{\mathbf{k}} = \Omega_{-\mathbf{k}}$. So if a system has both time-reversal and inversion symmetry, the Berry curvature is required to be simultaneously an even and odd function of momentum. This implies $\Omega_k = 0$.
4. The sum of the Chern numbers over all bands is zero, $\sum_n C^n = 0$.
5. If the crystal has additional crystal symmetries (these are always unitary) then the Berry curvature has extra symmetry constraints.

a. Example of a Chern Insulator model The first examples of Chern bands where found in the Quantum-Hall effect, but there is a very simple Chern insulators model in two dimensions. In real-space it is defined on a square lattice. We need to bands, so two orbital degrees of freedom will do $c_i^\dagger = (c_{Ai}^\dagger, c_{Bi}^\dagger)$. We define the model as [12, 26]

$$H = -t \sum_i \hat{c}_i^\dagger \frac{(\sigma_z - i\sigma_x)}{2} \hat{c}_{i+a\hat{x}} + \hat{c}_i^\dagger \frac{(\sigma_z - i\sigma_y)}{2} \hat{c}_{i+a\hat{y}} + \text{h.c.} + M \sum_i \hat{c}_i^\dagger \sigma_z \hat{c}_i \quad (142)$$

Imposing periodic boundary conditions we can go to Fourier space and find that the Hamiltonian is of the form $h_k = \mathbf{d}_k \cdot \boldsymbol{\sigma}$

$$\mathbf{d}_k = (t \sin k_x, t \sin k_y, M - t \cos k_x - t \cos k_y). \quad (143)$$

We may examine the (k_x, k_y) -plane to see where the gap vanishes. We notice this will occur at high symmetry points, and we wish to determine for which values of M/t the gap closes. When $M/t = -2$, the gap closes at (π, π) . When $M/t = 0$, the gap closes at $(0, \pi)$ and $(\pi, 0)$. When $M/t = 2$, the gap closes at $(0, 0)$. We this distinguish three phases as shown at the top figure in Fig. 11.

For this two-band model we can calculate the Chern number by directly computing

$$C = \frac{1}{4\pi} \int_{BZ} d^2k \hat{d}_{\mathbf{k}} \cdot (\partial_{k_x} \hat{d}_{\mathbf{k}} \times \partial_{k_y} \hat{d}_{\mathbf{k}}), \quad (144)$$

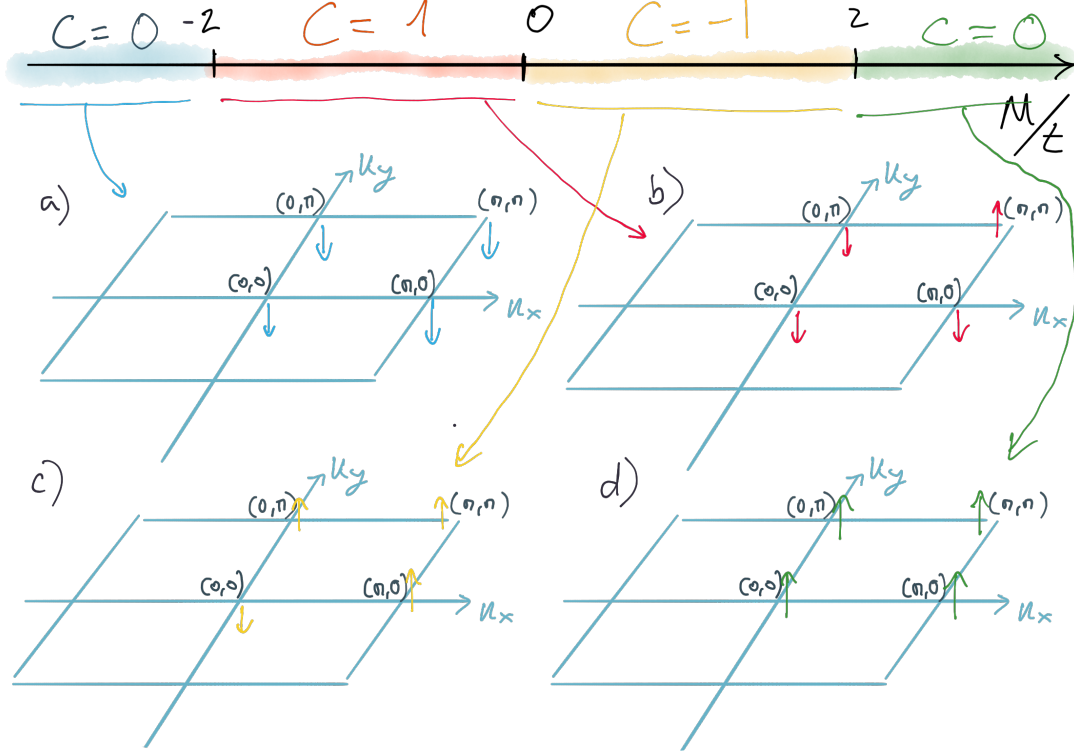


Figure 11. The different phases of the Chern insulator model (142) are distinguished by the change in orientation of the vector \hat{d}_k , defined in (143), at different high-symmetry points. These determine if we cover the two-sphere once or zero times ($C = \pm 1$ and $C = 0$, respectively).

but there is an easier, graphical way. The graphical way simply relies on checking \hat{d}_k at high-symmetry points and asking, considering the whole Brillouin zone, how many times the vector has covered the unit sphere (see Fig. 11).

We start with $\frac{M}{t} < -2$. We see from (143) that \hat{d}_k always points down. This means that \hat{d}_k never points to the northern hemisphere in the two-sphere. This implies that we never cover the surface of the two-sphere and thereby the Chern number of both bands is $C = 0$ (Fig. 11a).

However, when $-2 < \frac{M}{t} < 0$ we observe that \hat{d}_k around the point (π, π) , we see that \hat{d}_k now points upwards in the \hat{z} direction. Because \hat{d}_k has changed sign at this k -point, this implies that we cover the surface of the sphere once. Therefore the Chern number of the bands is $C_1 = -C_2 = 1$ (Fig. 11b). Once $\frac{M}{t} > 0$, \hat{d}_k will also change sign (and direction) at the points $(\pi, 0)$ and $(0, \pi)$. With three up vectors and one down, we now have Chern number of $C_1 = -C_2 = -1$ (Fig. 11c). The sign of the Chern number is a convention, but the difference between Chern numbers between the case $\frac{M}{t} \geq 0$ and the case with $-2 < \frac{M}{t} < 0$ is always two.

Finally, past $\frac{M}{t} = 2$, we see that $(0, 0)$ changes sign and we are again led to the case in which there is no winding around the sphere and the Chern numbers of all bands are zero again (Fig. 11d).

B. Chern number and the Hall Conductivity

Ok, so we know how to calculate Chern numbers. But what do they mean physically? They determine the Hall conductivity! Lets see why.

Consider a two-dimensional unit cell with side lengths of a_x and a_y . The Brillouin zone is therefore defined by the momenta $\frac{2\pi}{a_x}$ and $\frac{2\pi}{a_y}$. We recall that the Chern number is the integral of the Berry curvature over the Brillouin zone,

$$C_n = \frac{1}{2\pi} \iint dk_x dk_y \Omega_k^n. \quad (145)$$

To give us some physical intuition (and units!) it is useful to phrase this equation in terms of the Zak phase. Remember that the Zak phase is a 1D integral, so we need to cut the 2D Brillouin zone into different k_x

$$\Phi_n(k_x) = \int_0^{\frac{2\pi}{a_y}} dk_y \langle u_k^n | i\partial_{k_y} | u_k^n \rangle. \quad (146)$$

Remember that the Zak phase sets the average position of the Wannier center (in this case in the y direction), which also gives us some units

$$\bar{y}(k_x) = \frac{a_y}{2\pi} \Phi_n(k_x). \quad (147)$$

Now we remember that \bar{y} is a periodic coordinate, it gives us the Wannier center coordinate within a unit cell. It has to

return to itself upon changing k_x from 0 to 2π up to an integer, which is the Chern number

$$\Phi_n(k_x = 0) - \Phi_n(k_x = 2\pi/a_x) = 2\pi C_n. \quad (148)$$

Fig. 12 shows how schematically how each Wannier center moves as we move in k_x . There are two possibilities, either you traverse C unit cells in the y direction, or zero, if $C = 0$. This leads to two possibilities that are depicted in

So why is this related to the Hall effect? Imagine that we have an electric field in the x direction (E_x) acting on this Wannier center of charge. We can think of it as a semi-classical object, a wave-packet that changes its momentum because of Newton's law:

$$\hbar \dot{k}_x = -eE_x \quad (149)$$

To traverse the Brillouin zone in the x -direction, the wave packet has to undergo a change in momentum Δk_x given by

$$\Delta k_x = \frac{2\pi}{a_x},$$

which is achieved in a time (sometimes referred to as Bloch time)

$$\Delta t = \frac{\hbar}{ea_x E_x}.$$

Now we combine this with the knowledge that the change in the average position, $\Delta \bar{y}$, is an integer multiple of the Chern number. By combining (147) and (148)

$$\Delta \bar{y}_n = a_y C_n. \quad (150)$$

Then, the average velocity in the y -direction is

$$\langle v_y \rangle = \frac{\Delta \bar{y}}{\Delta t} = \frac{C a_x a_y e E_x}{\hbar}. \quad (151)$$

To compute the Hall conductivity σ_{xy} we need to look at the current density in the j_y direction, since by definition $j_y = \sigma_{xy} E_x$. The average current density is

$$\langle j_y^n \rangle = \frac{e}{a_x a_y} \langle v_y \rangle \quad (152)$$

$$= \frac{e}{a_x a_y} \frac{C_n a_x a_y}{\hbar} e E_x \quad (153)$$

$$= \frac{C_n e^2 E_x}{\hbar} = \sigma_{xy}, \quad (154)$$

So the Chern number determines the Hall conductivity. By the definition of Chern number we also learn that $\sigma_{yx} = -\sigma_{xy}$. We also learn that $\sigma_{xy} = 0$ if time-reversal symmetry is present, since this implies $C_n = 0$. Also, while we derived this result semi-classically (because we used (149) rather than deriving the current quantum mechanically) it holds quantum mechanically. You can find a derivation in standard text-books, e.g. [12, 15].

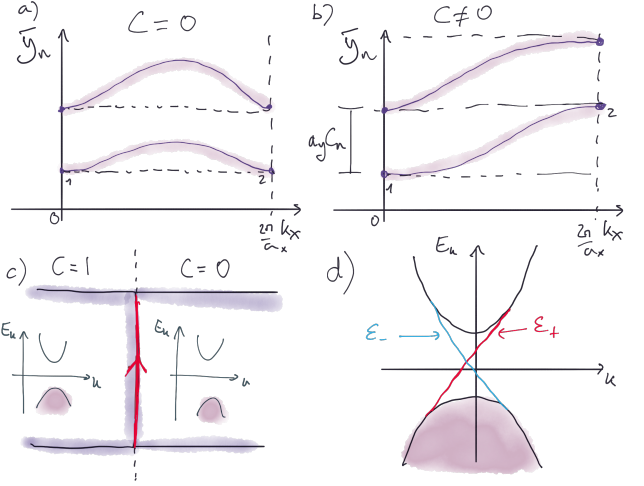


Figure 12. a and b show the average position of the Wannier center \bar{y}_n as we move in k_x . For a non-trivial band ($C_n \neq 0$) each Wannier center moves one unit cell when k_x changes from 0 to $2\pi/a$. c shows that the interface of two Hall insulators hosts a chiral edge mode. d shows that each edge has only one normalizable solution and they counterpropagate.

We derived the Hall conductivity for a given (filled) band n . In general, the total Hall conductivity is the sum of all filled states[27]:

$$\sigma_{xy} = \frac{e^2}{\hbar} \sum_n \int_{BZ} \frac{d\mathbf{k}}{(2\pi)^2} \Omega_{\mathbf{k}}^n n_f(\epsilon_{\mathbf{k}}^n - \mu) \quad (155)$$

where $n_f(\epsilon_{\mathbf{k}}^n)$ is the Fermi-Dirac distribution function. This integral in general is not quantized. It is only when we have an insulator, i.e. all filled bands have $n_f(\epsilon_{\mathbf{k}}^n) = 1$ and all empty bands satisfy $n_f(\epsilon_{\mathbf{k}}^n) = 0$, when the Hall conductivity is quantized

$$\sigma_{xy} = \frac{e^2}{\hbar} \sum_{n \in \text{occ}} \int_{BZ} \frac{d\mathbf{k}}{(2\pi)^2} \Omega_{\mathbf{k}}^n = \frac{e^2}{\hbar} \sum_{n \in \text{occ}} C_n \quad (156)$$

C. Bulk-boundary correspondence: Chiral boundary modes

Do Chern insulators have edge states? Indeed, as happened in 1D whenever two phases with different topological invariants are placed next to each other there is something interesting happening at the boundary. In the case of two Chern insulators with different Chern number we are about to find that it is a chiral edge mode (Fig. 12c).

Suppose the change in Chern number occurs as a function of y (Fig. 12c). As in 1D our strategy will be expand our Hamiltonian around a high symmetry point, and vary a parameter (the mass) as a function of y . As introduced earlier, the Hamiltonian for our Chern insulator example is defined by

$$\mathbf{d}_{\mathbf{k}} = (t \sin k_x, t \sin k_y, M - t \cos k_x - t \cos k_y). \quad (157)$$

We want to consider an interface between the phase with $C = 0$ and $C = 1$, which happens, in parameter space at $M/t =$

–2. The transition is triggered by a gap closing at the point (π, π) , so it makes sense to expand this Hamiltonian around this momentum

$$h_{\mathbf{k} \approx (\pi, \pi)} = t(-p_x \sigma_x - p_x \sigma_y) - m \sigma_z. \quad (158)$$

with $m = -2 + \delta m$ and $p_i = (k_i - \pi)$ is the momentum close to (π, π) . We call this a Dirac equation, and its dispersion relation ($E^\pm = \sqrt{t^2 p_x^2 + m^2}$) a gapped Dirac cone. Now to model a boundary we can choose $m(y)$ to be a function that is $m < -2$ at $y \rightarrow -\infty$ and $0 > m > -1$ at $y \rightarrow +\infty$. This guarantees that we are building an interface between Chern insulator $C = 0$ and $C = 1$. Following our steps in deriving the edge modes of the SSH chain we can go to real space in the y direction to write:

$$\begin{pmatrix} m(y) & t(-p_x + \partial_y) \\ -t(p_x + \partial_y) & -m(y) \end{pmatrix} \psi_{p_x}(y) = E_{p_x} \psi_{p_x}(y) \quad (159)$$

We are looking for a normalizable solution. There are two mathematical solutions to this equation, which have dispersion $E_{p_x} = \pm t p_x$ and the form[10]

$$\psi_{p_x}^\pm(y) = e^{-i p_x x} e^{\pm \int_0^y dy' m(y')} \begin{pmatrix} 1 \\ \pm 1 \end{pmatrix} \quad (160)$$

Which one we pick depends on our choice of $m(y)$. We can model our transition by writing it as $m(y) = -2 + m_0 f(y)$ where $f(y)$ satisfies $f(y \rightarrow \pm\infty) = \pm 1$. Now if $m_0 > 0$ we are modelling an interface between a $C = 0$ insulator on the left, and a $C = 1$ insulator on the right, as shown in Fig. 12c. In this case, the only normalizable solution is $\psi_{p_x}^-(y)$. Conversely if $m_0 < 0$, we are modelling an interface between a $C = 1$ insulator on the left, and a $C = 0$ insulator on the right, and the only normalizable solution is $\psi_{p_x}^+(y)$. Since we can think of $m_0 > 0$ and $m_0 < 0$ as modeling opposite edges of the same systems our results are telling us that two opposing edges will have each one solution, either $\psi_{p_x}^-(y)$ or $\psi_{p_x}^+(y)$. These modes counter propagate with respect to each other with dispersion relation $E_{p_x} = -t p_x$ and $E_{p_x} = +t p_x$, respectively (see Fig. 12d). Since they only in one direction (their Fermi velocity is either positive or negative), we say that these modes are propagating chirally.

Some final notes. From this analysis we can already see that if the transition changed the Chern number by n units, there would be n edge states per edge. These cannot be removed, unless we destroy the topological phases by closing the bulk-gap. In this sense, even if there is no symmetry to protect this phase, we still have topological protection, since the Chern number cannot change so long as the phase is gapped.

D. 2D Quantum Spin-Hall insulators

After the Quantum Hall effect a long-sought goal was to realize topological phases without breaking time-reversal symmetry. This could achieve robust edge transport, but without requiring magnetic fields. It took long to realize that there

are two ingredients to realize this dream: i) strong-spin orbit coupling and ii) Kramers degeneracy.

To understand why strong-spin orbit coupling can act as a magnetic field in creating topological states we may first notice a peculiar thing of how the magnetic field couples to electrons. In minimal substitution, we consider \mathbf{p} to be replaced by $\mathbf{p} - e\mathbf{A}$. For a free particle with energy $\mathbf{p}^2/2m$ this means we need to consider $(\mathbf{p} - e\mathbf{A})^2$ which generates a term $\mathbf{p} \cdot \mathbf{A}$, among others. A magnetic field in the z direction, B_z can be written with the help of the gauge $\mathbf{A} = \frac{1}{2}(-B_z y, B_z x, 0)$ which allows us to write $\mathbf{p} \cdot \mathbf{A} = \frac{1}{2}B_z L_z$ where L_z is the z component of the orbital angular momentum of the electron $\mathbf{L} = \mathbf{r} \times \mathbf{p}$. This should remind you of spin-orbit coupling $\lambda_{\text{so}} \mathbf{L} \cdot \mathbf{S}$, but there are remarkable differences. First the magnetic field breaks time-reversal symmetry, as we can see by noting that in $\frac{1}{2}B_z L_z$ only L_z changes sign and the Hamiltonian is not invariant anymore. In contrast, $\mathbf{L} \cdot \mathbf{S}$ is time-reversal even because both \mathbf{L} and \mathbf{S} are odd under time-reversal, leaving the product invariant. Also, unlike the magnetic field, spin-orbit coupling can vary at the scale of the unit-cell, while the magnetic field is constant. The strength of spin-orbit coupling grows with heavier atoms (because it is a relativistic correction to the electron's motion).

We then might be tempted to think that we can take two Chern insulators, that are time-reversed copies of each other, and build a state that is time-reversal symmetric and topological. This is a good idea, but we need an extra ingredient to make it work. In a Chern insulator the chiral edge-states cannot back scatter, they are topologically robust. However if we make two that go on opposite directions, they can backscatter, open up a gap, and ruin our newly build topological material.

Here is where the second ingredient comes in. As we learned in III B 1, time-reversal symmetry is different for half-integer spins because the operator that represents it satisfies $T^2 = -1$. As a result, time-reversed states are orthogonal to each other, but there is even a more interesting property: now time-reversal symmetric perturbation can couple time-reversed states. To show this recall that time-reversal is an anti-unitary operator so it complex conjugates the scalar product $\langle T\psi_1 | T\psi_2 \rangle = \langle \psi_1 | \psi_2 \rangle^* = \langle \psi_2 | \psi_1 \rangle$. Similarly, it satisfies:

$$\langle T\psi_1 | \hat{H} | T\psi_2 \rangle = \langle \psi_1 | H | \psi_2 \rangle \quad (161)$$

Now let's assume that \hat{H} is a perturbation that is time-reversal symmetric, so it commutes with \hat{T} . This can be for example impurities or defects so long as they are not magnetic. Now take two conjugate pairs: $|\psi_2\rangle = \psi$ and $|\psi_1\rangle = T\psi$. Inserting them into the left-hand side of the previous equation

$$\langle T^2 \psi | \hat{H} | T\psi \rangle = -\langle \psi | H | \psi \rangle = -\langle \psi | TH | \psi \rangle \quad (162)$$

but the right-hand side of (161) is $\langle \psi | TH | \psi \rangle$ implying that $\langle T\psi | H | \psi \rangle = 0$ for a time-reversal symmetric perturbation H . This is an extremely strong result and signals that if we carry through with our idea of opposite Chern number insulators the edge states won't gap out, because they are Kramers pairs of each other!

Let's introduce a couple of realistic models that exemplify these features.

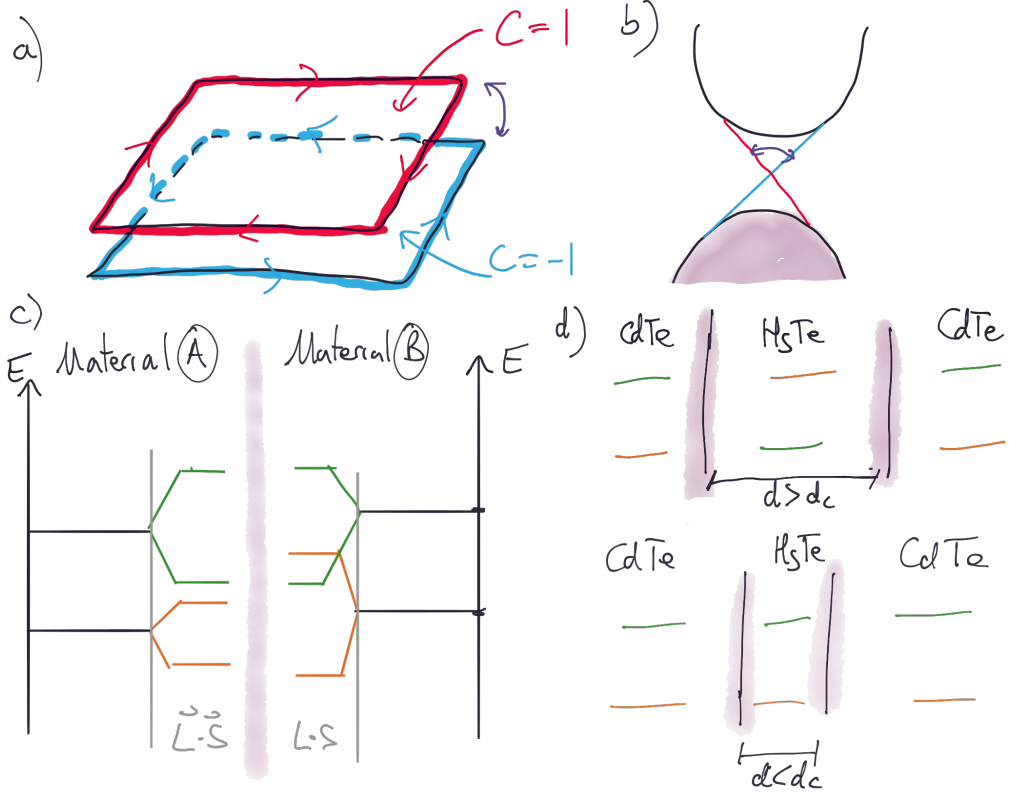


Figure 13. a) Two copies of Chern insulators related by time-reversal symmetry form a quantum spin-Hall effect. b) The backscattering between edge states (arrow) is forbidden by time-reversal symmetry. c) Large spin-orbit coupling can invert bands with different symmetry characters (green and orange). Interfacing a material with an inverted gap and a non-inverted material can lead to a topological edge state at the boundary. d) In CdTe/HgTe quantum wells, the width of the well d controls the gap inversion of HgTe, and thus whether or not there is a topological phase. .

a. *Example: Bernevig-Hughes-Zhang model* Bernevig, Hughes and Zhang [28] realized that a topological state protected by time-reversal symmetry could be realized in CdTe/HgTe quantum wells. To show this they wrote down the low energy model around the Γ point of both materials. There are four bands close to the Fermi level. These are given by one spinful s band with the spin being $\sigma = \uparrow, \downarrow$ and one spinful p band ($p_x + ip_y$). They showed that the symmetries of the crystal structure, and the particular interface relevant for experiment (which we will not discuss here) impose that the Hamiltonian takes the form

$$H = \sum_{\mathbf{k}} (c_{s\uparrow}^\dagger, c_{p\uparrow}^\dagger, c_{s\downarrow}^\dagger, c_{p\downarrow}^\dagger) \begin{pmatrix} h(\mathbf{k}) & 0_{2 \times 2} \\ 0_{2 \times 2} & h^*(-\mathbf{k}) \end{pmatrix} \begin{pmatrix} c_{s\uparrow} \\ c_{p\uparrow} \\ c_{s\downarrow} \\ c_{p\downarrow} \end{pmatrix} \quad (163)$$

defined by the 2×2 matrix $h(\mathbf{k}) = \epsilon_{\mathbf{k}} + \mathbf{d} \cdot \boldsymbol{\tau}$ with

$$\epsilon_{\mathbf{k}} = C - D(k_x^2 + k_y^2) \quad (164)$$

$$d_x + id_y = A(k_x + ik_y) \quad (165)$$

$$d_z = M - B(k_x^2 + k_y^2) \quad (166)$$

The parameters (A, B, C, D) are constants of the model, and depend on the material. For this particular system $B < 0$ and

the sign of M depends on the well's thickness: $M > 0$ for $d < d_c$ and $M < 0$ for $d > d_c$. Note that we have conveniently written the hamiltonian in a block structure, with each block representing each spin, and within each block a 2×2 structure that represents the orbital degree of freedom. In this basis, time-reversal symmetry is apparent if we chose it to be

$$\hat{T} = i\sigma_y K \otimes \tau_0 = \begin{pmatrix} i\sigma_y K & 0_{2 \times 2} \\ 0_{2 \times 2} & i\sigma_y K \end{pmatrix} \quad (167)$$

It is easy to check that each block does not have time-reversal symmetry, but since \hat{T} sends $h(\mathbf{k}) \rightarrow h^*(-\mathbf{k})$ and spin up to spin down we recover (163).

To find the topological properties of this model we focus on the vector $\hat{d}_{\mathbf{k}}$. We can again ask how many times does this vector cover the sphere as we go from $k = 0$ to $k \rightarrow \infty$. This is a bit of a quick and dirty way, because we know that there is a Brillouin zone. We will come back to this point later. For $k = 0$ we find that $\hat{d}_{\mathbf{k}=0} = (0, 0, \text{sgn}(M))$, while for $k \rightarrow \infty$ we have that $\hat{d}_{\mathbf{k}=0} = (0, 0, 1)$ (remember that $B < 0$). We see that if $M > 0$, the sphere is not covered, so $C = 0$, while if $M < 0$ the sphere is covered once, so $C = \pm 1$. The sign, is determined by how we cover it, this sign is opposite for $h_{\mathbf{k}}$ and $h^*_{-\mathbf{k}}$.

Excercise: Convince yourself by using expression (144) to compute the Chern number.

Thus, by our discussion of Chern insulators we conclude that this system is composed of two Chern insulators related by time-reversal symmetry. It is now possible to write the Hall conductivity:

$$\sigma_{xy} = \frac{1}{2}(\sigma_{xy}^{\uparrow} + \sigma_{xy}^{\downarrow}) = \frac{C_{\uparrow} + C_{\downarrow}}{2} \frac{e^2}{h} = 0 \quad (168)$$

The Hall conductivity is zero because $C_{\uparrow} = -C_{\downarrow}$. This should not surprise you: remember we showed that all systems with time-reversal symmetry have an odd Berry curvature which integrates to zero, resulting in a total Chern number of zero and thus $\sigma_{xy} = 0$.

However the *spin-Hall conductivity* need not be zero:

$$\sigma_{xy}^s = \frac{1}{2}(\sigma_{xy}^{\uparrow} - \sigma_{xy}^{\downarrow}) = \frac{C_{\uparrow} - C_{\downarrow}}{2} \frac{e^2}{h} \equiv C_s \frac{e^2}{h} = \frac{e^2}{h} \quad (169)$$

We have just found a new topological phase: The quantum spin-Hall insulator. This phase is characterized by a non-zero spin-Chern number $C_s = \frac{C_{\uparrow} - C_{\downarrow}}{2}$.

If you look at table V, you see that indeed with time-reversal symmetry that squares to -1 , in $d = 2$ there is class AIII, which has a topological invariant of \mathbb{Z}_2 . But if the spin-Hall conductivity is a sum of Chern numbers are Chern numbers are integers, why don't we have a classification $\mathbb{Z} \times \mathbb{Z}$?

The reason can be understood by recalling again the effect of time-reversal symmetry on the edges. If we have $C_s = 1$ we have two counter-propagating edge states that cannot back-scatter, per our arguments above. However, if we have $C_s = 2$ then we have four edge states. These can scatter by pairs, and thus can gap out. Therefore this is topologically equivalent to the case with $C_s = 0$. This is true for all even integers, so the only topologically distinct states are $C_s = 0, 1$, trivial and topological. The topological index is thus defined modulo 2, hence the \mathbb{Z}_2 classification. This index tells us how many pairs of edge states we have at the boundary, again an example of the bulk-boundary correspondence.

The spin-Hall conductivity is hard to measure directly. However, the above was confirmed in Molenkamp's group in Wurzburg by looking at edge conductance [29]. Since there are two edge states, they managed to observe a quantized conductance close to $2e^2/h$. Currently WTe₂ has shown to have an even more accurate quantization[30].

One last comment. We argued in terms of a continuum Hamiltonian. However, this is not entirely satisfactory, because continuum models can have Chern numbers that depend on how we regularize the Hamiltonian at $\mathbf{k} \rightarrow \infty$. You can see this by keeping only terms to order k , what Chern number would you get? If you are given a continuum hamiltonian, but don't have a lattice Hamiltonian, you can use a trick to regularize it and get a lattice Hamiltonian with the same topological properties. Simply trade $k_i \rightarrow \sin(k_i)$ and $k_i^2 \rightarrow 2(\cos(k_i) - 1)$. Close to Γ , these functions reduce back to the BHZ Hamiltonian, but away from the Brillouin zone center they will restore periodicity of the Brillouin zone.

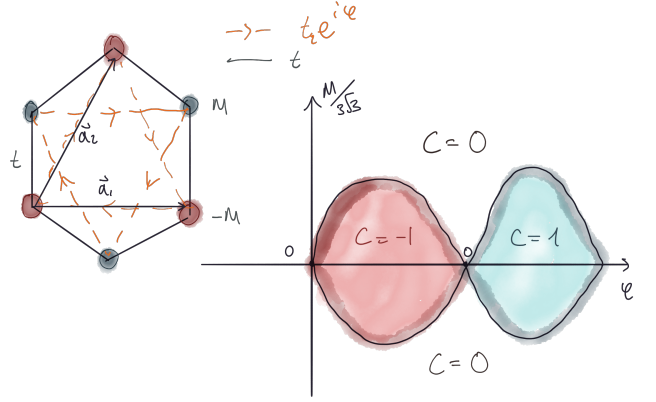


Figure 14. The Haldane model features complex second-nearest neighbour hoppings. The phase diagram has three phases distinguished by their Chern number. The Kane and Mele model is given by two time-reversed copies of the Haldane model. .

Excercise: Show that the substitution $k_i \rightarrow \sin(k_i)$ and $k_i^2 \rightarrow 2(\cos(k_i) - 1)$ maps $h(\mathbf{k})$ to a Chern insulator model we discussed in the previous section. Compute its Chern number (e.g. using (144) or graphically) for $M > 0$ and $M < 0$, with fixed A, B , and show that the topological properties are determined by the parameter $(M - 4B)/2B$. Show that at $M = 0$ there is a gap closing at the Γ point, which changes the Chern number from $C = 0$ to $C = 1$.

b. Example: Kane-Mele model = 2 Copies of Haldane model Around the same time as the above model was proposed, Kane and Mele [31] realized that you can build a topological phase without breaking time-reversal symmetry in graphene. They proposed to think about a honeycomb lattice with large spin-orbit coupling. Their model reduces to two Chern insulator models related by time-reversal symmetry.

The Chern-insulator model in the honeycomb lattice is known as the Haldane model [32] (see Fig. 14). It features the normal nearest-neighbour hoppings of graphene, but also a complex second-nearest neighbour hopping.

$$H = \sum_{\langle ij \rangle} t_1 c_{iA}^\dagger c_{jB} \quad (170)$$

$$+ \sum_{\langle\langle ij \rangle\rangle} t_2 e^{i\phi} c_{iA}^\dagger c_{jA} + t_2 e^{-i\phi} c_{iB}^\dagger c_{jB} \quad (171)$$

$$+ m \sum_i c_{iA}^\dagger c_{iA} - c_{iB}^\dagger c_{iB} \quad (172)$$

In momentum space it can also be written as $h_{\text{Hald}}(\mathbf{k}) = \epsilon_{\mathbf{k}} + \mathbf{d} \cdot \boldsymbol{\tau}$ with

$$d_{\mathbf{k}}^x = t_1 (\cos(\mathbf{k} \cdot \mathbf{a}_1) + \cos(\mathbf{k} \cdot \mathbf{a}_2) + 1) \quad (173)$$

$$d_{\mathbf{k}}^y = t_1 (\sin(\mathbf{k} \cdot \mathbf{a}_1) + \sin(\mathbf{k} \cdot \mathbf{a}_2)) \quad (174)$$

$$d_{\mathbf{k}}^z = m + 2t_2 \sin \phi (\sin(\mathbf{k} \cdot \mathbf{a}_1) - \sin(\mathbf{k} \cdot \mathbf{a}_2) - \sin(\mathbf{k} \cdot (\mathbf{a}_1 - \mathbf{a}_2))) \quad (175)$$

with $\mathbf{a}_{1,2}$ the lattice vectors of the triangular lattice, which defines the Kane and Mele Hamiltonian:

$$h_{KM}(\mathbf{k}) = \begin{pmatrix} h_{\text{Hald}}(\mathbf{k}) & 0 \\ 0 & h_{\text{Hald}}^*(-\mathbf{k}) \end{pmatrix} \quad (176)$$

The insight of Kane and Mele was to predict that this model is a good description of graphene with spin-orbit coupling [31]. Unfortunately, spin-orbit coupling is small in graphene, as it goes with the atomic number Z , and carbon is a very light element.

VI. 3D TOPOLOGICAL INSULATORS IN CLASS AIII

We now want to move on and consider 3D topological insulators in class AIII, also protected by time-reversal symmetry with $\hat{T}^2 = -1$. There is a simple way by thinking about SSH models in momentum space. Later we will define a lattice model in the square lattice that has topological properties.

To start, we will be assuming time-reversal symmetry ($U_T h_k^* U_T = h_{-k}$) with $\hat{T}^2 = -1$, chiral symmetry ($U_S h_k U_S = -h_k$) and inversion symmetry ($U_I h_k U_I = h_{-k}$). Later we will relax all but time-reversal and argue that the topological surface states are robust.

We are going to construct our 3D topological insulator using the 1D SSH chain. Consider the 1D-SSH Hamiltonian (71), but doubled, a copy for each spin \uparrow, \downarrow . This means that for a finite system we are going to have a pair of end-states at zero energy, because of chiral symmetry. Note also, that each of the energy bands are two-fold degenerate. This is because the two bands ε_k^\uparrow and ε_k^\downarrow go to $\varepsilon_{-k}^\downarrow$ and $\varepsilon_{-k}^\uparrow$, respectively, under time-reversal, and then to ε_k^\downarrow and ε_k^\uparrow , respectively, under inversion. Since we return to the same bands, we conclude that the combination of time-reversal and inversion must make the bands degenerate (see Fig. 15a).

Now we are ready to construct the 3D TI. Consider a square Brillouin zone, which has eight time-reversal (and inversion) invariant momenta: $(0, 0, 0), \{(\pi, 0, 0)\}, \{(\pi, \pi, 0)\}, (\pi, \pi, \pi)$, where the braces indicate all permutations. Now we are going to demand that at certain momenta our Hamiltonian for the 3D topological insulator, $H^{\text{TI}}(k_x, k_y, k_z)$ recovers the SSH chain Hamiltonian

$$H^{\text{TI}}(0, 0, k_z) = h_{\text{SSH}}^{\text{top}}(k_z) \quad (177)$$

$$H^{\text{TI}}(0, \pi, k_z) = H^{\text{TI}}(\pi, 0, k_z) = H^{\text{TI}}(\pi, \pi, k_z) = h_{\text{SSH}}^{\text{tr}}(k_z) \quad (178)$$

where $h_{\text{SSH}}^{\text{top}}(k_z)$ and $h_{\text{SSH}}^{\text{tr}}(k_z)$ are SSH Hamiltonians with parameters such that they are in the topological or trivial phases. This requirement can be schematically drawn as in Fig. 15b. We have also drawn the inversion symmetry eigenvalues of the lowest band. Notice that the product of all inversion eigenvalues (we take only one of the two degenerate bands) is odd. This already motivates the definition of an invariant, just as we did with the SSH chain:

$$\nu = \prod_{n \in \text{occ}} \prod_{k \in \text{TRIM}} \xi_{k, 2n} = \pm 1 \quad (179)$$

The $2n$ takes into account that we only need one of the two degenerate bands to calculate the invariant. This invariant, defined for the first time by Fu and Kane[33], signals the presence ($\nu = -1$) of absence ($\nu = 1$) of robust surface states.

To see why, let's open the chain in the z direction, and use periodic boundary conditions in k_x and k_y . This will result in a spectrum shown in Fig. 15c). If we look at the top surface for example, we find at Γ two degenerate zero modes. These are there because at Γ we imposed a topological SSH Hamiltonian with chiral symmetry, and we have two because we have two spin species. Now what happens to these zero modes as we move away from Γ ? We can find out by simply counting. At Γ there must be $N - 1$ conduction states, and $N - 1$ valence states because our slab is length N in the z direction and we have two zero modes. These sum to $2N$, as they should (two spin states and a chain of length N). Now, at the corners of the Brillouin zone, we also have $2N$ states, but no zero modes, so they must be distributed with N in the conduction band and N in the valence band. We conclude that changing momentum from Γ to the corner, the degeneracy of the zero modes is lifted, and they disperse away from zero by pairs.

To convince yourself think about symmetries. The only interpolation between Γ that respects the symmetries is the one shown because time-reversal imposes $\epsilon_k = \epsilon_{-k}$, and chiral symmetry imposes that for every state at ϵ_k there is a state at $-\epsilon_k$. Since this occurs in any direction in the (k_x, k_y) plane, we conclude there is a cone-like state at the surface. We have found the Dirac cone.

But we already know that the dispersion of the Dirac cone should be, to lowest order in momentum linear! Back in III B 1c we showed that the linear dispersion is compatible with time-reversal symmetry, so long we don't have a gap $m\sigma_z$ term, and provided it is composed by real spin. In fact, it is only time-reversal symmetry that protects this state. If we would have removed chiral symmetry but keep time-reversal symmetry, the only possibility is that the cone can move up and down, but never gap out. The only reason we used inversion is to simplify the calculation of the topological invariant. However this is not required; you can define the topological invariant as a generalization of polarization in three-dimensions[34, 35]

$$\theta = \sum_{\text{occ}} \int \frac{d^3k}{(4\pi)} \epsilon^{ijl} \text{Tr} \left[A_i \partial_{k_j} A_l - i \frac{2}{3} A_i A_j A_l \right] \quad (180)$$

where $A_i^{nm} = \langle u_k^n | \partial_{k_i} u_k^m \rangle$ is the non-abelian (multiband) Berry connection, and the trace is over occupied bands. As you can see, this is a much more complicated expression to evaluate than Eq. (179), but the advantage is that it delivers the topological invariant even when inversion symmetry is absent.

Lastly, we can understand why it is a \mathbb{Z}_2 invariant and not a \mathbb{Z} invariant much in the same way as the QSH. For an even number of Dirac cones, scattering processes are allowed between different Dirac cones, gapping them out. However, for an odd number of surface states, the Dirac can gap out by pairs, but will always leave one behind, protected by Kramers degeneracy.

Topological insulators have been observed in many materials. Bi_2Se_3 is a textbook topological insulator with inversion

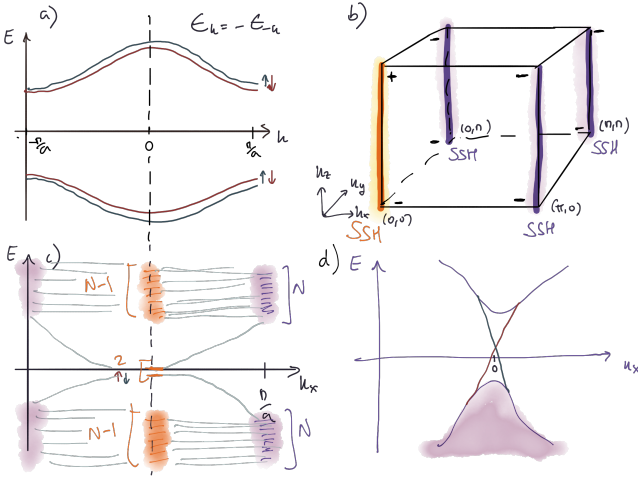


Figure 15. Construction of a 3D TI from SSH chains. a) The spin-full SSH chain has two doubly degenerate bands, one for each spin. b) To construct a 3D topological insulator we first require that the full Hamiltonian recovers the SSH Hamiltonian at certain momenta. The symmetry eigenvalues are also indicated. c) The full Hamiltonian with open boundary conditions interpolates between different SSH models, and thus lifts the degeneracy of the edge states. d) In the continuum limit, these are the Dirac surface states, which cross at Γ . They need not be pinned at zero energy. .

symmetry. It was predicted by the group of S.-C. Zhang in Stanford and the Dirac cone was observed by Hasan's group in Princeton [1]. It was an exciting development because it was the first time a topological phase was observed in three-dimensions, and it did not require magnetic fields!

a. Example a. 3D topological insulator model We now give for concreteness a lattice model for a three-dimensional topological insulator. You can find a very complete discussion here [34]. The matrix conventions are taken from here[36].

The model is defined on a square lattice with two orbitals and two spins per site by a Hamiltonian

$$H = t \sum_i c_i^\dagger \left(\frac{\Gamma_0 - i\Gamma_x}{2} \right) c_{i+\hat{x}} + c_i^\dagger \left(\frac{\Gamma_0 - i\Gamma_y}{2} \right) c_{i+\hat{y}} + c_i^\dagger \left(\frac{\Gamma_0 - i\Gamma_z}{2} \right) c_{i+\hat{z}} + \text{h.c.} + M \sum_i c_i^\dagger \Gamma_0 c_i \quad (181)$$

where $c_i^\dagger = (c_{i,A\uparrow}^\dagger, c_{i,A\downarrow}^\dagger, c_{i,B\uparrow}^\dagger, c_{i,B\downarrow}^\dagger)$, $\Gamma_0 = \sigma_x \otimes s_0$, $\Gamma_x = \sigma_z \otimes s_y$, $\Gamma_y = \sigma_z \otimes s_x$, $\Gamma_z = \sigma_y \otimes s_0$ where s_i and σ_i are Pauli matrices describing the spin and orbital degree of freedom, respectively. In momentum space this Hamiltonian takes the form

$$H = t \sum_{\mathbf{k}} c_{\mathbf{k}}^\dagger h_{\mathbf{k}}^{\text{TI}} c_{\mathbf{k}} \quad (182)$$

$$h_{\mathbf{k}}^{\text{TI}} = t \sin k_x \Gamma_x + t \sin k_y \Gamma_y + t \sin k_z \Gamma_z \quad (183)$$

$$+ (M - \sum_i \cos k_i) \Gamma_0 \quad (184)$$

Exercise Show that it has inversion symmetry and use it to calculate the topological invariant. In the parameter regime where

it is topological, diagonalize this model with open boundary conditions and find the Dirac cone. You can diagonalize it numerically, or expand close to a high-symmetry point and use a space dependent mass $M(z)$.

VII. WEYL SEMIMETALS

To describe topological semimetals we are going to go the opposite way we usually go: first we will describe the continuum Hamiltonian, and then use a trick to define a lattice model. We consider a 2×2 Hamiltonian in three-dimensions of the form

$$h_+ = v_F k_x \sigma_x + v_F k_y \sigma_y + v_F k_z \sigma_z \quad (185)$$

$$= v_F \mathbf{k} \cdot \boldsymbol{\sigma} \quad (186)$$

The eigenvalues are $E_{\pm} = \pm v_F |\mathbf{k}|$, so it forms a cone in momentum space, the Weyl cone (see Fig. ??a). We notice the two bands touch at a point, the Weyl node, and we may ask if we can lift this degeneracy by adding any perturbation to (187) with the sub-space of 2×2 matrices. This subspace is completely spanned by the Pauli matrices σ_i and the identity σ_0 so, to lowest order in moment, the most general perturbation we can add is

$$h_p = h_+ + \mathbf{b} \cdot \boldsymbol{\sigma} + b_0 \cdot \boldsymbol{\sigma} \quad (187)$$

with \mathbf{b} a constant vector and b_0 a constant. We observe that there is no way to lift the degeneracy. It is simple to see why: \mathbf{b} can be reabsorbed by a definition of the momentum, and b_0 by a definition of the zero of energies. In other words, we can shift the cone around, but we will not open up a gap!

Is this protection topological? Lets calculate the Berry curvature of one of the eigenstates of h_+ . We gave the expression of the Berry curvature of a 2×2 hamiltonian in terms of the vector $\hat{d}_{\mathbf{k}}$, which in our case is $\hat{d}_{\mathbf{k}} = \hat{k} = \mathbf{k}/|\mathbf{k}| = \mathbf{k}/k$ (it is the integrand of Eq. 144)

$$\vec{\Omega}_k^{n=1} = \vec{\nabla} \times \vec{A}_k^{n=1} \quad (188)$$

$$= \hat{d}_{\mathbf{k}} \cdot (\partial_{k_x} \hat{d}_{\mathbf{k}} \times \partial_{k_y} \hat{d}_{\mathbf{k}}) = \frac{\mathbf{k}}{2k^3} \quad (189)$$

we thus find that for the lowest band $n = 1$ the Berry curvature looks like a monopole (see Fig. ??b), emanating from the origin. Now, here we see a problem. If the Hamiltonian (187) was to be obtained from a tight-binding model, we would have the problem that the Berry curvature would always be outgoing, and cannot be periodic in the Brillouin zone. We have to conclude that there must be another monopole, a sink, that compensates for this Chern flux. The simplest way to compensate for this flux is to have another monopole, with opposite flux

$$h_- = -v_F \mathbf{k} \cdot \boldsymbol{\sigma} \quad (190)$$

It is not difficult to show that the Berry curvature is exactly opposite from that of h_+ . Thus the simplest low energy Hamiltonian of a Weyl semimetal is

$$h_{\text{Weyl}} = \begin{pmatrix} h_+ & 0 \\ 0 & h_- \end{pmatrix} \quad (191)$$

It is topological in the sense that only by coupling these two monopoles to each other, we may open a gap, since each 2×2 Hamiltonian h_{\pm} is stable independently. But what allows us to have zero in the off-diagonals?

VIII. ACKNOWLEDGEMENTS

I am grateful to K. Driscoll who drafted the first version of these notes.

Appendix A: Useful relations

Completeness relation:

$$\sum_{\mathbf{x}} e^{-i(\mathbf{q}-\mathbf{q}')\mathbf{x}} = N\delta\mathbf{q}\mathbf{q}' \quad (\text{A1})$$

Sums to integrals:

$$\sum_{\mathbf{k}} = \frac{V}{2\pi^3} \int d^3k \quad (\text{A2})$$

where $V = N * V_{\text{cell}}$ and $N = N_x N_y N_z$ is the number of primitive cells.

Appendix B: Kramers theorem

We want to show that $T|\phi\rangle$ and $|\phi\rangle$ are orthogonal. Consider:

$$\langle T\phi|T\psi\rangle = \sum_{mpr} (U_{mp}\mathcal{K}\phi_p)^* U_{mr}\mathcal{K}\phi_r \quad (\text{B1})$$

$$= \sum_{mpr} U_{mp}^* \phi_p U_{mr} \phi_r^* \quad (\text{B2})$$

$$= \sum_{pr} \phi_p \delta_{pr} \phi_r^* \quad (\text{B3})$$

$$= \langle \psi | \phi \rangle \quad (\text{B4})$$

If $|\psi\rangle = T|\phi\rangle$ and $T^2 = -1$ we obtain $\langle T\phi|\phi\rangle = -\langle T\phi|\phi\rangle = 0$, so the two states are orthogonal. They have the same energy, per Eq. (34).

Appendix C: Pauli matrices

$$\sigma_x = \begin{pmatrix} 0 & 1 \\ 1 & 0 \end{pmatrix}$$

$$\sigma_x = \begin{pmatrix} 0 & -i \\ i & 0 \end{pmatrix}$$

$$\sigma_x = \begin{pmatrix} 1 & 0 \\ 0 & -1 \end{pmatrix}$$

These matrices satisfy the following properties: $\sigma_i^2 = 1$, $\sigma_i \sigma_j = 2\delta_{ij}$ and $\sigma_i \sigma_j = 0$ and $[\sigma_i, \sigma_j] = 2i\epsilon_{abc}\sigma_c$ and $\sigma_i \sigma_j = 0$, where ϵ_{abc} is the Levi-Civita symbol.

Appendix D: Exact results for two-band Hamiltonians

Any first-quantized two-band Bloch Hamiltonian can be written as

$$h = \vec{d}_k \cdot \vec{\sigma} + \varepsilon_k \cdot \mathbb{1} \quad (\text{D1})$$

$$(\text{D2})$$

The energies can be calculated exactly by squaring the Hamiltonian and using the properties of Pauli matrices:

$$E_k^{\pm} = \pm|\vec{d}_k| + \varepsilon_k. \quad (\text{D3})$$

The exact eigenvectors take the form:

$$|+k\rangle = \frac{1}{\sqrt{2|\vec{d}|(d_z + |\vec{d}|)}} \begin{pmatrix} d_z + |\vec{d}| \\ d_x + id_y \end{pmatrix} \quad (\text{D4})$$

$$|-k\rangle = \frac{1}{\sqrt{2|\vec{d}|(d_z + |\vec{d}|)}} \begin{pmatrix} id_y - id_x \\ d_z + |\vec{d}| \end{pmatrix} \quad (\text{D5})$$

The normalized Hamiltonian $h = \frac{\vec{d}}{|\vec{d}|} \cdot \vec{\sigma} \equiv \hat{d} \cdot \vec{\sigma}$ can be parametrized in spherical coordinates as

$$\hat{d} = (\sin \theta \cos \phi, \sin \theta \sin \phi, \cos \theta) \quad (\text{D6})$$

$$(\text{D7})$$

The corresponding eigenvalues are ± 1 with eigenvectors

$$|+k\rangle = \begin{pmatrix} \cos \frac{\theta}{2} e^{-i\phi} \\ \sin \frac{\theta}{2} \end{pmatrix} \quad (\text{D8})$$

$$|-k\rangle = \begin{pmatrix} \sin \frac{\theta}{2} e^{-i\phi} \\ -\cos \frac{\theta}{2} \end{pmatrix} \quad (\text{D9})$$

[1] M Z Hasan and Charles L Kane, “Colloquium: Topological insulators,” *Reviews of Modern Physics* **82**, 3045–3067 (2010).

[2] Xiao-Liang Qi and Shou-Cheng Zhang, “Topological insulators

- and superconductors,” *Rev. Mod. Phys.* **83**, 1057–1110 (2011).
- [3] N P Armitage, E J Mele, and Ashvin Vishwanath, “Weyl and Dirac semimetals in three-dimensional solids,” *Reviews of Modern Physics* **90**, 1443 (2018).
- [4] Tomoki Ozawa, Hannah M. Price, Alberto Amo, Nathan Goldman, Mohammad Hafezi, Ling Lu, Mikael C. Rechtsman, David Schuster, Jonathan Simon, Oded Zilberberg, and Iacopo Carusotto, “Topological photonics,” *Rev. Mod. Phys.* **91**, 015006 (2019).
- [5] Valerio Peri, Marc Serra-Garcia, Roni Ilan, and Sebastian D Huber, “Axial-field-induced chiral channels in an acoustic Weyl system,” *Nature Physics* **15**, 357–361 (2019).
- [6] Xiao-Gang Wen, “Colloquium: Zoo of quantum-topological phases of matter,” *Rev. Mod. Phys.* **89**, 041004 (2017).
- [7] Adolfo G. Grushin, “Topological phases of amorphous matter,” arXiv, arXiv:2010.02851 (2020), arXiv:2010.02851 [cond-mat.dis-nn].
- [8] H Bruus and K Flensberg, *Many-Body Quantum Theory in Condensed Matter Physics* (Oxford Graduate Texts, 2004).
- [9] W. P. Su, J. R. Schrieffer, and A. J. Heeger, “Solitons in polyacetylene,” *Phys. Rev. Lett.* **42**, 1698–1701 (1979).
- [10] Andreas W W Ludwig, “Topological phases: classification of topological insulators and superconductors of non-interacting fermions, and beyond,” *Physica Scripta* **T168**, 014001 (2015).
- [11] Ching-Kai Chiu, Jeffrey C Y Teo, Andreas P Schnyder, and Shinsei Ryu, “Classification of topological quantum matter with symmetries,” *Reviews of Modern Physics* **88**, 035005 (2016).
- [12] B. A. Bernevig, *Topological insulators and Superconductors* (Princeton Press, 2013).
- [13] To achieve the last step expand the exponential.
- [14] JJ Sakurai, *Modern Quantum Mechanics* (Addison-Wesley Pub, 1994).
- [15] D. Vanderbilt, *Berry Phases in electronic theory* (Cambridge University Press, 2018).
- [16] N. R. Cooper, J. Dalibard, and I. B. Spielman, “Topological bands for ultracold atoms,” *Rev. Mod. Phys.* **91**, 015005 (2019).
- [17] János K. Asbóth, László Oroszlány, and András Pályi, “A short course on topological insulators,” *Lecture Notes in Physics* (2016), 10.1007/978-3-319-25607-8.
- [18] R. Jackiw and C. Rebbi, “Solitons with fermion number $1/2$,” *Phys. Rev. D* **13**, 3398–3409 (1976).
- [19] D. J. Thouless, “Quantization of particle transport,” *Phys. Rev. B* **27**, 6083–6087 (1983).
- [20] M Lohse, C Schweizer, O Zilberberg, Monika Aidelsburger, and I Bloch, “A Thouless quantum pump with ultracold bosonic atoms in an optical superlattice,” *Nature Physics* **12**, 350–354 (2016).
- [21] Shuta Nakajima, Takafumi Tomita, Shintaro Taie, Tomohiro Ichinose, Hideki Ozawa, Lei Wang, Matthias Troyer, and Yoshiro Takahashi, “Topological Thouless pumping of ultracold fermions,” *Nature Physics* **12**, 296–300 (2016).
- [22] Jason Alicea, “New directions in the pursuit of Majorana fermions in solid state systems,” *Reports on Progress in Physics* **75**, 076501 (2012).
- [23] N R Cooper, J Dalibard, and I B Spielman, “Topological bands for ultracold atoms,” *Reviews of Modern Physics* **91**, 015005 (2019).
- [24] Frank Schindler, Barry Bradlyn, Mark H Fischer, and Titus Neupert, “Pairing Obstructions in Topological Superconductors,” *Physical Review Letters* **124**, 247001 (2020).
- [25] Xiao-Liang Qi, Yong-Shi Wu, and Shou-Cheng Zhang, “Topological quantization of the spin hall effect in two-dimensional paramagnetic semiconductors,” *Phys. Rev. B* **74**, 085308 (2006).
- [26] Yang-Le Wu, B. Andrei Bernevig, and N. Regnault, “Zoology of fractional chern insulators,” *Phys. Rev. B* **85**, 075116 (2012).
- [27] F. D. M. Haldane, “Berry curvature on the fermi surface: Anomalous hall effect as a topological fermi-liquid property,” *Phys. Rev. Lett.* **93**, 206602 (2004).
- [28] B. Andrei Bernevig, Taylor L. Hughes, and Shou-Cheng Zhang, “Quantum Spin Hall Effect and Topological Phase Transition in HgTe Quantum Wells,” *Science* **314**, 1757–1761 (2006), cond-mat/0611399.
- [29] Markus Konig, Steffen Wiedmann, Christoph Brüne, Andreas Roth, Hartmut Buhmann, Laurens W. Molenkamp, Xiao-Liang Qi, and Shou-Cheng Zhang, “Quantum Spin Hall Insulator State in HgTe Quantum Wells,” *Science* **318**, 766–770 (2007), 0710.0582.
- [30] Sanfeng Wu, Valla Fatemi, Quinn D. Gibson, Kenji Watanabe, Takashi Taniguchi, Robert J. Cava, and Pablo Jarillo-Herrero, “Observation of the quantum spin Hall effect up to 100 kelvin in a monolayer crystal,” *Science* **359**, 76–79 (2018), 1711.03584.
- [31] C. L. Kane and E. J. Mele, “Quantum spin hall effect in graphene,” *Phys. Rev. Lett.* **95**, 226801 (2005).
- [32] F. D. M. Haldane, “Model for a quantum hall effect without landau levels: Condensed-matter realization of the ‘parity anomaly’,” *Phys. Rev. Lett.* **61**, 2015–2018 (1988).
- [33] Liang Fu and Charles L Kane, “Topological insulators with inversion symmetry,” *Phys. Rev. B* **76**, 45302 (2007).
- [34] Xiao Liang Qi, Taylor L Hughes, and Shou-Cheng Zhang, “Topological field theory of time-reversal invariant insulators,” *Physical Review B* **78**, 195424 (2008).
- [35] Andrew M Essin, Joel E Moore, and David Vanderbilt, “Magnetolectric Polarizability and Axion Electrodynamics in Crystalline Insulators,” *Physical Review Letters* **102**, 146805 (2009).
- [36] Adolfo G Grushin, Jorn W F Venderbos, and Jens H Bardarson, “Coexistence of Fermi arcs with two-dimensional gapless Dirac states,” *Phys. Rev. B* **91**, 121109 (2015-03).